CDF/PHYS/ELECTROWEAK/CDFR/8506
Version 2.0
March 26, 2007

Measurement of $Z\gamma$ Production using 1 fb^{-1} of CDF RUN II Data

J. Deng, A. Goshaw, B. Heinemann, J. Kist , C. Lester, A. Nagano, T. Phillips

Berkeley, Duke and Tsukuba University

Abstract

This note describes a measurement of $p\bar{p} \rightarrow l^+l^- + \gamma$ + X production using CEM-CEM or CEM-PEM electrons and CMUP/CMX muons with an additional high P_T track. A loose electron selection criteria was developed to maximize the data sample and minimize the bias to selected events. The electron and muon efficiencies and backgrounds were validated by measurements of the cross sections for inclusive Z production. The details of the loose lepton selection criteria and the inclusive Z cross section measurement are described in CDF note 8505 and 8758. The central photon selection uses standard Joint Physics group cuts. The cross sections for $p\bar{p} \rightarrow l^+l^- + \gamma$ + X production are measured for photon E_T > 7 GeV and ΔR(l-γ)>0.7. The cross sections and kinematic distributions are compared to Standard Model predictions.

Contents

1 Introduction

Previous studies of Zγ production have been limited by statistics of the data sample. In this note we describe a measurement using 1.07 fb^{-1} of integrated $p\bar{p}$ luminosity, and a loose Z selection criteria to maximize statistics. This results in a cross section measurement with statistical, systematic and luminosity uncertainties approximately equal, and a data set over ten times the size used in CDF's previous publication[3] .

The analysis selects $p\bar{p} \rightarrow l^+l^- + \gamma + \mathrm{X}$ events with CEM-CEM or CEM-PEM electrons, and CMUP/CMX muons with an additional high P_T track. A central high E_T photon is selected with $\eta < 1.0$. The measurement is inclusive over the recoil system X. The final event selection requires photon $E_T > 7$ GeV, ΔR(l-γ)>0.7, and $M_{ll} > 40$ GeV/c^2. These data are used to measure Zγ production properties where the photon is from either initial state radiation off the colliding quarks or from final state radiation in Z$\rightarrow e^+e^-\gamma$. Other processes with a photon from a direct tri-linear ZZγ or an excited Z' decay are absent in the Standard Model. The measured cross sections and kinematic distributions are compared to predictions of a LO electroweak calculation[4] with corrections obtained from a partial NLO calculation.

The measurement described in this note draws heavily on CDF note 8505 and 8758 where the electron and muon selection criteria, ID efficiencies and backgrounds are presented. These are validated by a measurement of the inclusive Z boson production cross section. The analysis presented here uses the same Z/$\gamma^* \rightarrow l^+l^-$ selection, but also requires the presence of a photon in the central detector region($\eta < 1.1$) with E_T > 7 GeV.

2 Data sets, Good run list, Triggers, Luminosity

The high Pt electron datasets bhel0d, bhel0h and bhel0i are used in this analysis. The total integrated luminosity of the data is 1.07 fb^{-1}.

All the runs are required to be in the version 13 good run list for Top/EWK/Exotics electron, no silicon. Data collected during the COT compromised period (from Feb 2004 to May 2004) is not used in this analysis.

All selected events are required to fire the ELECTRON_CENTRAL_18 trigger or the Z_NOTRACK trigger. The calculation of the trigger efficiencies is described in section 7.

See the Z selection note [1] for more details on the datasets and the trigger efficiency measurements.

3 Baur $Z\gamma$ MC Samples

3.1 Baur $Z\gamma$ Samples

The Baur LO ZGAMMA program[4] is used to generate $Z\gamma$ samples for the $Z\gamma$ analysis. The parton level cuts used for generating $Z\gamma$ Baur MC samples are listed in table 1.

variables	Sample
P_T^γ(GeV/c)	> 4.0
$\Delta R(e,\gamma)$	> 0.2
M_{ee} (GeV/c^2)	> 20.0
$M_{ee\gamma}$ (GeV/c^2)	> 20.0
M_{gen} (GeV/c^2)	> 1.0
P_T^e (GeV/c)	> 0.0
$\vert\eta^\gamma\vert$	< 10.0
$\vert\eta^e\vert$	< 10.0
PDF	CTEQ 5L
$\sigma_{LO}(pb)$	5.8
	Gen5 (Gen6)
Number of Events	3.2M (3.3M)
Lum(fb^{-1})	551. (568.)

Table 1: Parton level cuts used for generating $Z\gamma$ Baur MC samples.

The parton level generator is then coupled to PYTHIA for modeling the parton showering, hadronization and the underlying event. The radiation setting for the PYTHIA interface is discussed in detail in [5]. After this, the events are passed through the CDF detector simulation.

Table 2 lists the Pythia $Z\gamma$ Duke Ntuples used in this analysis. A total of 6M MC events are generated.

dataset	run range	Offline Release Version	Duke Ntuple Production	Number of Events
rewk03	141544 - 186598	Pythia 5.3.3ewk	6.1.2	3.2 M
rewk23	190753 - 212133	Pythia 6.1.4mc	6.1.4	3.3 M

Table 2: Baur $Z\gamma$ MC samples.

3.2 High Order QCD Correction – K-Factor

The Baur NLO ZGAMMA program is used to calculate the higher order QCD corrections for the $Z\gamma$ production. The NLO correction factor is defined as:

$$k = \frac{\sigma_{NLO}}{\sigma_{LO}}. \qquad (1)$$

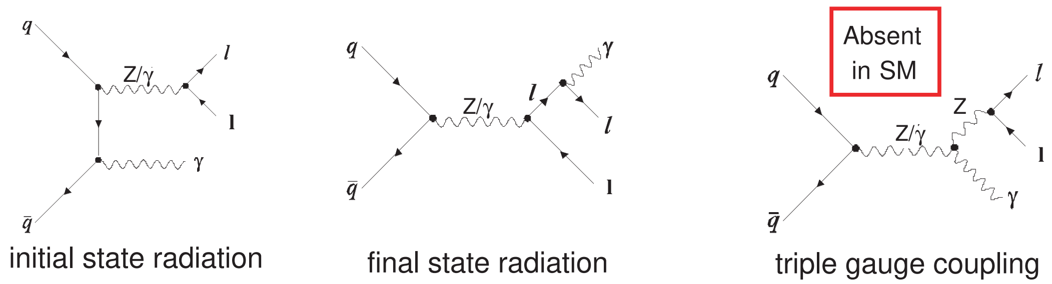

Figure 1: Tree level Feynman graphs for the $Z\gamma$ production.

The k-factor is obtained as following[3]:

- The LO/NLO prgrams contains different channels(see Figure 1):
  - LO Baur $Z\gamma$ program: contains ISR and FSR channels
  - NLO Baur $Z\gamma$ program: contains **ONLY** ISR channels
- To distinguish $p\bar{p} \to Z \to e^+e^-\gamma$ and $p\bar{p} \to Z\gamma \to e^+e^-\gamma$:
  - use $M_{ee\gamma}$ cut at 100 GeV/c^2
- Apply different corrections to these two subsets
- $p\bar{p} \to Z \to e^+e^-\gamma$, Events with $M_{ee\gamma} < 100$ GeV/c^2 :
  - Applied the inclusive Z NLO correction of **1.36**[3]
- $p\bar{p} \to Z\gamma \to e^+e^-\gamma$, Events with $M_{ee\gamma} \geq 100$ GeV/c^2 :

$$k(Z\gamma\ , E_T^\gamma\ ) = 1.46 - 0.00073 \cdot E_T^\gamma\ - 0.125 \cdot e^{-0.062 \cdot E_T^\gamma} \qquad [3]$$

- The Et dependent k-factor is applied to MC sample event by event.

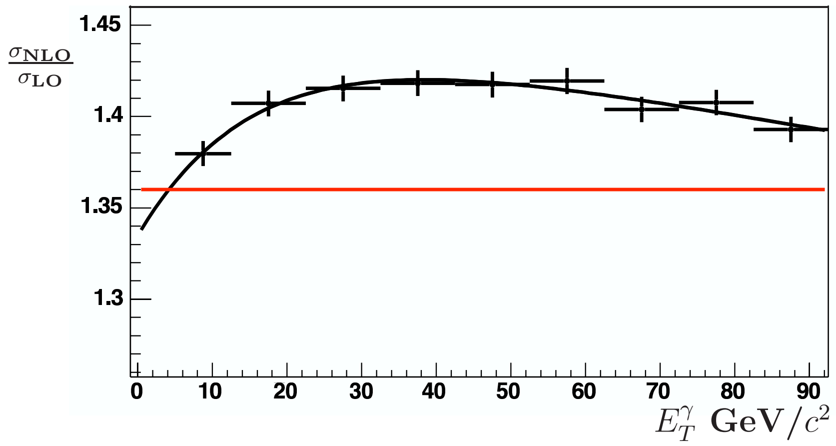

Figure 2: The ratio of the NLO cross-section to that of the corresponding LO cross-section, calculated with NLO Baur $Z\gamma$ program. LO cross-section calculation uses CTEQ5L LO PDFs, NLO calculation used CTEQ5M NLO PDFs. The red line shows the k-factor for the inclusive Z production. CDF note 7996[3].

4 Photon Selection

4.1 Central Photon ID Cuts

In this section, details on the Central Photon selection are given. Table 3 lists photon variables and cuts used to identify a photon object in the event. Joint Physics baseline analysis cuts for high Pt photons(v2.3)[6] are used.

Central photon ID variables[6]:

- raw E:
  The total amount of energy for a photon is obtained directly using the Emcluster method.
  It uses the 2-tower sum from:
  emobj_alg::CEMFourMomentum::TwoTower(emObject,usetrack =false).e().
  (compare to Electron:
  emobj_alg::CEMFourMomentum::TwoTower(emObject,usetrack =true).e().)

- E:
  The energy is then corrected to the CES position(x and z) using the em_alg::cemcorr.

Variables	Cut	variable in Duke Ntuple
ECorr		pho_rawEnergy/energyCorr
EtCorr	>7	ECorr* sin(θ)
$\|cesX\|$	< 21 cm	cempho_cesX
$\|cesZ\|$	$9 < \|cesZ\| < 230$ cm	cempho_cesZ
Had/Em	< 0.125 || < 0.055 + 0.00045 * ECorr	pho_hadem
IsoEtCorr	EtCorr < 20: < 0.1 * EtCorr EtCorr $\geq$ 20: < 2.0 + 0.02 * (EtCorr - 20.0)	
Chi2 (Strips + Wires)/2	< 20	cempho_cesChi2Strip cempho_cesChi2Wire
N track(N3D)	≤ 1	pho_n3d
Track Pt	< 1.0 + 0.005 * EtCorr	pho_pt
Cone 0.4 Track Iso	< 2.0 + 0.005 * EtCorr	
2nd CES cluster E*sin(θ)	(both strip and wire E individually) EtCorr < 18: < 0.14 * EtCorr EtCorr $\geq$ 18: < 2.4 + 0.01 * EtCorr	cempho_cesStrip(Wire)E2

Table 3: Central Photon ID cuts

- E_T :
  The transverse component of E, corrected to the Vertex Z of the photon.

- cesX and cesZ:
  The photon position inside an electromagnetic calorimeter tower. It is measured by the CES detector.

- Had/Em:
  Ratio of the hadronic/electromagnetic energy.

- IsoEtCorr:
  Calorimeter isolation energy in cone 0.4. The isolation energy is corrected to the photon sin(θ). It is then corrected for leakage energy and number of vertices(quality>=12 ZVertex collection).

- Chi2:
  A χ^2 fit of the CES shower profile (strip or wire) to the same profile of the test beam electrons.

- N track (N3D):
  The number of tracks, pointing to the photon energy cluster

- Track Pt:
  Pt of the highest pt track, pointing to the photon energy cluster.

- Cone 0.4 track Iso
  Track isolation energy is sum over all tracks within 5 cm of the photon vertex in 0.4 Cone.

- Second CES cluster E*sin(θ):
  Energy of the second strip(wire) cluster.

- photon Vertex Z
  For our $Z\gamma$ analysis, there will be two electrons in the events. The vertex information of the central electrons is used to determine the vertex Z of the central photons. If there is a vertex within 5cm of the central electrons in the events, that vertex is used as the photon vertex, otherwise the vertex Z of the highest Et central electron is used.

5 $Z\gamma$ Event Selection

5.1 Electron Selection

Table 4 and 5 list the electron selection in the central and forward region, respectively. For more details on the electron selection and ID efficiency measurement, see the Z selection note[1].

Variables	Cut	variable in Duke Ntuple
Region	CEM ($\|\eta\| < 1.1$)	EMCLST_ele_det==0
COT track	satisfy loose track quality requirements	
E_T	≥ 20	EMCLST_ele_std_Et
$TrackP_T$	≥ 10	
E_{had}/E_{em}	$\leq 0.055 + 0.00045 \cdot$ EMCLST_ele_std_E	EMCLST_ele_std_hadEm
Conversion	!= 1	CEMCLST_cem_convflag
CES fiducial	= 1	EMCLST_ele_fidEleShrMax
Iso(R=0.4)/E_T	no Iso cut applied yet	
	≤ 0.1 (Joint Physics standard cut)	EMCLST_ele_std_calIsoRatio
	≤ 0.3 (Loose Isolation cut)	
Lshr	≤ 0.4	CEMCLST_cem_std_lshr
$\|\Delta Z\|$	≤ 8	CEMCLST_cem_std_deltaZ

Table 4: Event selection: Loose Central Electron ID Cuts. The text in red shows the cut that is different to the Joint Physics Standard ID cut.

5.2 $Z\gamma$ Event Selection in the Central Photon Channel

Z selection:

Variables	Cut	variable in Duke Ntuple
Region	PEM ($1.1 \leq \|\eta\| < 3.6$)	EMCLST_ele_det==1
PES 2D Eta	$1.2 \leq \|\eta\| \leq 2.8$	PEMCLST_pem_pes2dGlobalEta
$CorrE_T$	≥ 20	
E_{had}/E_{em}	≤ 0.05	EMCLST_ele_std_hadEm
PEM 3x3 chi2	$\leq 25.$	PEMCLST_pem_std_pem3x3Chi
Iso(R=0.4)/E_T	no Iso cut applied yet	
	≤ 0.1 (standard Joint Physics cut)	EMCLST_ele_std_calIsoRatio
	≤ 0.3 (loose isolation cut)	

Table 5: Loose plug electron ID cuts in this analysis, the text in red shows the cut that is different to the Joint Physics Standard ID cut.

- For each event, require at least two high Pt electrons:
  - CC: two opposite-sign central loose electrons(table 4)
  - CP: central loose electron(table 4) and plug loose electron(table 5)
- Both electrons: loose isolation(IsoR $<$ 0.3)
- At least one electron: tight isolation(IsoR $<$ 0.1)

Photon selection:

- For each event, require at least one high Et photon:
  - Joint Physics Central Photon Baseline Cuts(table 3)
  - Photon $E_T > 7$ GeV

$Z\gamma$ event selection:

- $\Delta R_{e\gamma}$ >0.7: no effect on signal from anomalous couplings
- M_{ee} >40 GeV/c^2
- Invariant $ee\gamma$ Mass:
  - Control Region(FSR dominate): $M_{ee\gamma} \leq$100 GeV/c^2
  - probe anomalous couplings(ISR dominate): $M_{ee\gamma}$ >100 GeV/c^2

6 ID Efficiencies and Scale Factors

6.1 Total $Z\gamma$ Event Selection Efficiency

The total selection efficiency for data is given as:

$$\epsilon_{\rm tot}^{\rm Data} = \epsilon_{\rm Zid}^{\rm Data} \times \epsilon_{\gamma\rm id}^{\rm Data} \times \epsilon_{\rm vtx} \times \epsilon_{\rm trg} \tag{2}$$

where:

- ϵ_{Zid} is the Z selection efficiency. $\epsilon_{Zid} = \epsilon_{e1} \times \epsilon_{e2}$
- $\epsilon_{\gamma id}$ is the photon selection efficiency.
- ϵ_{trg} is the total trigger efficiency.
- ϵ_{vtx} is the efficiency of the $Z_0 \leq 60cm$ requirement.

The total selection efficiency for MC is given as:

$$\epsilon_{\rm tot}^{\rm MC} = \epsilon_{\rm Zid}^{\rm MC} \times \epsilon_{\gamma\rm id}^{\rm MC} \tag{3}$$

The data to MC scale factor is then:

$$SF = \epsilon_{\rm tot}^{\rm Data}/\epsilon_{\rm tot}^{\rm MC} = SF_{Zid} \times SF_{\gamma id} \times \epsilon_{\rm vtx} \times \epsilon_{\rm trg} \tag{4}$$

The trigger efficiency is applied as a weight to MC sample event by event(see Sec. 7).

The total data to MC scale factors are listed in tables 14 - 22.

6.2 Scale Factor for Photon ID Selection

The Photon ID scale factors are measured here[7].

For Gen5 data(run $\leq$ 186598), the photon ID efficiency and scale factors are listed in table 6.

Efficiency(%)	Data	MC	Scale Factor
Central	93.35 $\pm$ 0.69	92.61 $\pm$ 0.16	1.01 $\pm$ 0.71% (stat.) $\pm$ 1% (syst.)
Plug	77.85 $\pm$ 0.57	87.21 $\pm$ 0.11	0.89 $\pm$ 0.59% (stat.) $\pm$ 1% (syst.)

Table 6: Total photon ID efficiencies and scale factors for Gen5(run $\leq$ 186598) data [7].

For Gen6 data(run > 186598), the photon ID efficiency and scale factors are listed in table 7.

Efficiency(%)	Data	MC	Scale Factor
Central	90.85 ± 0.73	92.61 ± 0.16	0.98 ± 0.75% (stat.) ± 1% (syst.)
Plug	80.08 ± 0.51	87.21 ± 0.11	0.92 ± 0.52% (stat.) ± 1% (syst.)

Table 7: Total photon ID efficiencies and scale factors for Gen6 (run > 186598) data [7].

6.3 Scale Factor for Electron Selection

The measurement of the electron ID efficiencies and scale factors are described in detail in the Z selection note[1].

6.3.1 Central Electron ID Efficiency

The efficiencies and scale factors for the full $1fb^{-1}$ dataset are summarized in table 8.

dataset	Efficiency	Data	MC	Scale Factor
bhel0d	Loose ID	0.961	0.959	1.003
	Loose Iso	0.997	0.997	1.000
	Tight Iso	0.980	0.981	0.999
	Tight ID	0.874	0.882	0.991
bhel0h	Loose ID	0.957	0.958	0.999
	Loose Iso	0.997	0.997	1.000
	Tight Iso	0.977	0.979	0.998
	Tight ID	0.871	0.884	0.985
bhel0i	Loose ID	0.953	0.957	0.996
	Loose Iso	0.997	0.997	1.000
	Tight Iso	0.978	0.977	1.001
	Tight ID	0.868	0.883	0.983

Table 8: The efficiencies and scale factors for central electron, bhel0d/0h/0i dataset.

6.3.2 Plug Electron ID Efficiency

The efficiencies and scale factors for the full $1fb^{-1}$ dataset are summarized in table 9.

7 $Z\gamma$ Trigger Efficiency

Two triggers, ELECTRON_CENTRAL_18 trigger and Z_NOTRACK trigger, are used in the analysis. In the $Z\gamma$ event selection, either ELECTRON_CENTRAL_18 trigger or Z_NOTRACK trigger is required to be fired in the event.

dataset	Efficiency	Data	MC	Scale Factor
bhel0d	Loose ID	0.921	0.939	0.981
	Loose Iso	0.998	0.999	0.999
	Tight Iso	0.978	0.986	0.992
	Tight ID	0.965	0.981	0.984
bhel0h	Loose ID	0.912	0.930	0.981
	Loose Iso	0.999	0.999	1.000
	Tight Iso	0.970	0.983	0.987
	Tight ID	0.970	0.978	0.992
bhel0i	Loose ID	0.905	0.927	0.977
	Loose Iso	0.998	0.999	1.000
	Tight Iso	0.969	0.980	0.988
	Tight ID	0.968	0.978	0.990

Table 9: The efficiencies and scale factors for plug electron, bhel0d/0h/0i dataset.

7.1 Total ELECTRON_CENTRAL_18 Trigger Efficiency

The total ELECTRON_CENTRAL_18 trigger efficiency in $Z\gamma$ event selection can be determined as following:

- CC Z events: $\epsilon^{Ele18} = 1 - (1 - \epsilon(Pt_1)) \times (1 - \epsilon(Pt_2))$
- CP Z events: $\epsilon^{Ele18} = \epsilon(Pt)$
- PP Z events: $\epsilon^{Ele18} = 0$
- Pt is the central electron track Pt
- $\epsilon(Pt)$ is the ELECTRON_CENTRAL_18 trigger efficiency as a function of central electron Pt.

7.2 Total Z_NOTRACK Trigger Efficiency

The total Z_NOTRACK trigger efficiency in Z event selection can be determined as following:

- CC Z events: $\epsilon^{Z\_NOTRACK} = \epsilon_{Cen}(Et_1) \cdot \epsilon_{Cen}(Et_2)$
- CP Z events: $\epsilon^{Z\_NOTRACK} = \epsilon_{Cen}(Et_1) \cdot \epsilon_{Plug}(Et_2)$
- PP Z events: $\epsilon^{Z\_NOTRACK} = \epsilon_{Plug}(Et_1) \cdot \epsilon_{Plug}(Et_2)$
- Et_1 and Et_2 are the Et of the electrons.

For $Z\gamma$ events, the ZNOTRACK trigger could be fired by either ee or eγ. The photon must be included in the trigger efficiency calculation. The total trigger efficiency for $Z\gamma$ events with a central photon, is determined as following:

- Calculate efficiencies $\epsilon_i(Et_i)$, i = 1, 2, 3
  where Et_i is the Et of the electrons/photon.
- $\epsilon^{Z\_NOTRACK} = 1 - (1 - \epsilon_1 \cdot \epsilon_2) \times (1 - \epsilon_1 \cdot \epsilon_3) \times (1 - \epsilon_2 \cdot \epsilon_3)$

7.3 Total Trigger Efficiency

Finally, the total trigger efficiency in the $Z\gamma$ event selection is given as:
$\epsilon_{trig} = 1 - (1 - \epsilon^{Ele18}) \times (1 - \epsilon^{Z\_NOTRACK})$
This is then applied to MC sample event by event as a trigger efficiency weight.

As shown in the Z selection note[1], the total trigger efficiency (photon not included) is

- CC Z selection, $\sim$ 100%.
- CP Z selection, $\sim$ 99.6%.
- PP Z selection, $\sim$ 96%.

More details on trigger efficiency measurements are given in the Z selection note[1].

8 QCD Background

The $Z\gamma$ production channel is very clean, with only two significant background sources. The main background is from Z + jet events, where the jet fakes a photon. A second background source is γ + fake Z events, where a jet fakes an electron. The estimated backgrounds are shown in tables 11 - 13. The Z + Jet background is $\sim$10%, and the γ + fake Z background $\sim$ 4%.

8.1 Z + Jet QCD Background

8.1.1 Photon Fake Rate

Using jet triggered samples, the photon fake rate is obtained as following[3]:

- raw fake rate $P_{raw}(E_T^{jet})$: the fraction of jets which pass the photon selection criteria in the jet triggered samples.

$$P_{raw}(E_T^{jet}) = \frac{N_{\gamma-candidate}}{N_{jet}} \tag{5}$$

- The jet samples contains two categories of photon:
  - Prompt Photon: from the hard scattering process, or radiated off a quark
  - "fake" photon: any photons due to the decay of a meson(e.g. π_0)
- Find the fraction of fake photons in the jet samples:
  - Prompt photon contamination F_γ:

$$F_\gamma = \frac{N_\gamma}{N_\gamma + N_{jet\to\gamma}} = \frac{N_\gamma}{N_{\gamma-candidate}} \tag{6}$$

  - fraction of fake photons in the photon candidates sample, F_{jet}:

$$F_{jet} = \frac{N_{jet\to\gamma}}{N_\gamma + N_{jet\to\gamma}} = \frac{N_{jet\to\gamma}}{N_{\gamma-candidate}} = 1 - F_\gamma \tag{7}$$

- true fake rate $P_{jet\to\gamma}(E_T^{jet})$: correct prompt photon contamination in the jet samples

$$P_{jet\to\gamma}(E_T^{jet}) = \frac{N_{jet\to\gamma}}{N_{jet}} = \frac{N_{\gamma-candidate}}{N_{jet}} \times \frac{N_{jet\to\gamma}}{N_{\gamma-candidate}} = P_{raw}(E_T^{jet}) \times F_{jet} \tag{8}$$

Figure 3 shows the raw fake rate measured with 200 pb^{-1} of data.

Figure 3: $P_{raw}(E_T^{jet})$ versus E_T^{jet} comparing JET 20 (open points) and JET 50, JET 70 and JET 100 data (full points). CDF note 7996.

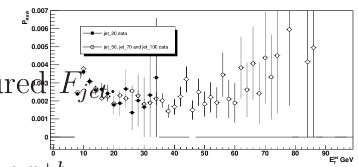

Figure 4 shows the measured F_{jet}.

$$F_{jet} = \frac{N_{jet\to\gamma}}{N_{\gamma-candidate}} = e^{-a\cdot x+b} + c, \qquad a = 0.207, b = 0.0668, c = 0.0888.$$

Figure 5 shows the true fake rate measured with 200 pb^{-1} of data.

$$P_{jet\to\gamma}(E_T^{jet}) = P_{raw}(E_T^{jet}) \times F_{jet} = e^{-a\cdot x+b} + c, \;\; a = 0.1526, b = 2.3969, c = 0.40369$$

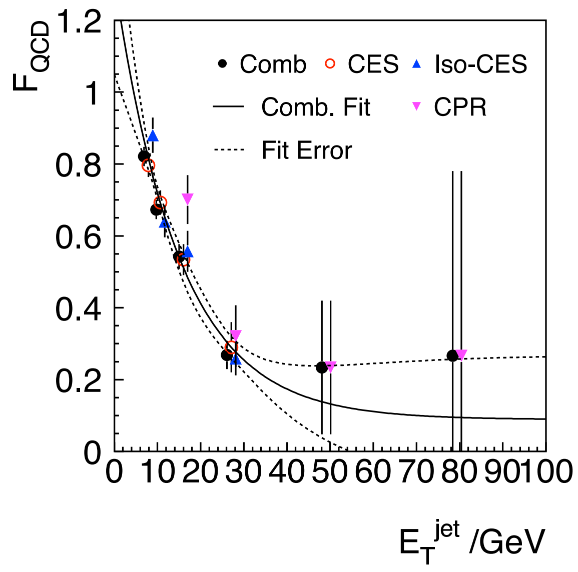

Figure 4: F_{jet} as a function of E_T^{jet}. "Comb": combination of the three methods. CDF note 7996.

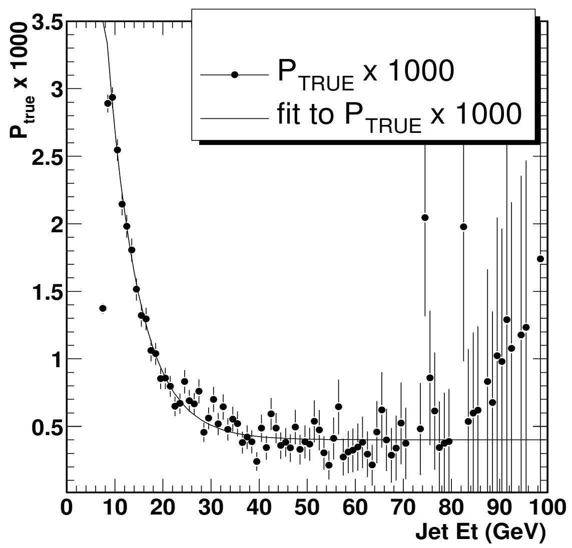

Figure 5: The corrected true fake rate $P_{jet\to\gamma}(E_T^{jet})$ for the 345th jet sample. CDF note 7996.

8.1.2 Fragmentation Function

The energy calculation for photons and jets are different:

- Photon energy: electromagnetic energy of a cluster of TWO towers
- Jet energy: all electromagnetic and hadronic energy within a cone of $\Delta R < 0.4$

We define a fragmentation function $z(E_T^{jet}, E_T^{\gamma})$:

- The probability that a jet of E_T^{jet} will be measured as E_T^{γ} .
- CDF note 7996, 200 pb^{-1} of data.
- The distribution is shown in figure 6.
- Gaussian fit: z = 0.934$\pm$ 0.001 and σ_z = 0.0428 $\pm$ 0.0008

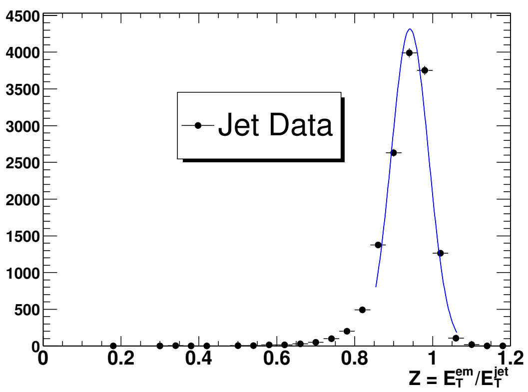

Figure 6: The distribution of $z = E_T^{\gamma} \; / \; E_T^{jet}$ in the jet triggered data samples. Shown is a Gaussian fit to the distribution. CDF note 7996.

8.1.3 Estimate Z + Jet QCD Background

We apply the jet $\rightarrow$ photon fake rate to the Z + jet events in the electron-triggered data sample, where the jet has $|\eta| < 1.1$ and $\Delta R_{ej} > 0.7$. The number of background events from jets faking photons is given as[3]:

$$
\begin{aligned}
N_{BG}(E_T^{\gamma}) &= \int_0^{N_{jet}(Z)} P^Z_{jet\rightarrow\gamma}(E_T^{jet}) \times dN_Z/dE_T^{jet} \times z(E_T^{jet}, E_T^{\gamma})dE_T^{jet} \qquad (9)\\
&= \int_0^{N_{jet}(Z)} P^j_{jet\rightarrow\gamma}(E_T^{jet}) \times \frac{dN_Z/dE_T^{jet}}{dN_{jet}/dE_T^{jet}} dN_{jet}/dE_T^{jet} \times z(E_T^{jet}, E_T^{\gamma})dE_T^{jet}
\end{aligned}
$$

where,

- $P^{j}_{jet\rightarrow\gamma}(E_T^{jet})$: probability of a jet faking a photon for jets in the jet sample
- $P^{Z}_{jet\rightarrow\gamma}(E_T^{jet})$: probability of a jet faking a photon for jets in the Z sample
- $z(E_T^{jet}, E_T^{\gamma})$: probability of a jet of $E_T^{jet}$to be measured as E_T^{γ} .
- dN_Z/dE_T^{jet}: E_T^{jet}distribution in Z sample
- dN_{jet}/dE_T^{jet}: E_T^{jet}distribution in a jet triggered sample
- $\frac{dN_Z/dE_T^{jet}}{dN_{jet}/dE_T^{jet}}$ term cancels if the distributions in the two samples are the same.
- "345th" jet sample:
  The sample of jets of the 3rd, 4th, 5th etc. highest E_T jets. The 345th jet in the jet samples has a very similar E_T^{jet}distribution as that in the Z sample. This sample is used to measure $P_{jet\rightarrow\gamma}(E_T^{jet})$.

8.2 γ + Jet QCD Background

We assume that the fake Z QCD background in the $Z\gamma$ sample scales as in the inclusive Z sample. The fake Z QCD background in the $Z\gamma$ sample is estimated as:

- $N_{Z\gamma}^{Bkg} = N_Z^{Bkg} * R$
  where,
  - N_Z^{Bkg} is the estimated QCD background in the inclusive Z cross section measurement(see the Z selection note[1])
  - $R = \frac{N_{FakeZ\gamma}}{N_{FakeZ}}$ is obtained from the fake Z background template (electron-antielectron sample)
- for CC, estimate 1.8 ± 1.3 background events(see Table 13)
- Cross check with same-sign method: observe 3 same-sign CC eeγ events
- for CP, estimate 12.1 ± 8.4 background events(see Table 13)

9 Systematic Uncertainties

To calculate the uncertainties on $Z\gamma$ cross section measurement:

- Write the cross section calculation in the form:

$$\sigma = \frac{N_d - \Sigma N_{bi}}{D}$$

  where:

- N_d = number of selected $Z\gamma$ events(data)
- N_{bi} = estimated background of type i
- D = $A \cdot \epsilon_{MC} \cdot SF \cdot \int \mathcal{L}dt$
- Propagating uncertainties in N_d, N_{bi} and D:

$$\begin{aligned}(\frac{\Delta\sigma}{\sigma})^2 = (\frac{N_d}{N_d - \Sigma N_{bi}})^2 \cdot (\frac{\Delta N_d}{N_d})^2 \\ +(\frac{N_{bi}}{N_d - \Sigma N_{bi}})^2 \cdot (\frac{\Delta N_{bi}}{N_{bi}})^2 \\ +(\frac{\Delta D}{D})^2\end{aligned}$$

Cross section denominator error:

- D = $A \cdot \epsilon_{MC} \cdot SF \cdot \int \mathcal{L}dt$
- Next expand $\frac{\Delta D}{D}$:

$$\begin{aligned}(\frac{\Delta D}{D})^2 = (\frac{\Delta(L\epsilon_{z<60})}{L\epsilon_{z<60}})^2 + (\frac{\Delta A_{ee\gamma}}{A_{ee\gamma}})^2 \\ +(\frac{\Delta\epsilon_{trig}}{\epsilon_{trig}})^2 + (\frac{\Delta ID_{SF}}{ID_{SF}})^2\end{aligned}$$

- Finally, expand $\frac{\Delta A_{ee\gamma}}{A_{ee\gamma}}$:

$$(\frac{\Delta A_{ee\gamma}}{A_{ee\gamma}})^2 = (\frac{\Delta A_{ee\gamma}}{A_{ee\gamma}})^2_{QCD} + (\frac{\Delta A_{ee\gamma}}{A_{ee\gamma}})^2_{PDF} + (\frac{\Delta A_{ee\gamma}}{A_{ee\gamma}})^2_{EM}$$

  where:

  - $(\frac{\Delta A_{ee\gamma}}{A_{ee\gamma}})^2_{QCD}$: uncertainties due to parton level generation(LO vs NLO)
  - $(\frac{\Delta A_{ee\gamma}}{A_{ee\gamma}})^2_{PDF}$: PDF errors
  - $(\frac{\Delta A_{ee\gamma}}{A_{ee\gamma}})^2$: uncertainty due to central/plug EM energy scale

Table 10 summaries all the uncertainties considered for the $Z\gamma$ cross section.

Notes on uncertainties:

- From $200pb^{-1}$ measurement[3]:
  - Z + Jet background: 35% (average)
  - γ energy scale: 3%
  - Acceptance(LO vs NLO) : 1%

Source	%	% effect on $\sigma(Z_{CC}\gamma)$	%	% effect on $\sigma(Z_{CP}\gamma)$	CC	CP
Signal Statistics	7.4	8.0	7.0	8.5		
Luminosity	5.8	5.8	5.8	5.8		
γ energy scale	3	2	3	2	x	x
γ conversion rate uncertainty	2	2	2	2	x	x
γ ID efficiency	3	3	3	3	x	x
Electron energy scale	1	2.5	1	2.5	x	x
Central electron ID efficiency	1	2	1	1	2x	x
Plug electron ID efficiency	–	–	2	2		x
Trig efficiency	1	1	1	1	x	x
Acceptance	1	1	1	1	x	x
γ + Jet background	63	0.7	45	3.2	x	x
Z + Jet background	38	2.5	39	5.9	x	x
Total Systematic Uncertainty		6.0		8.6		

Table 10: A summary of the uncertainties for the FSR+ISR $ee\gamma$ cross-section calculation and their correlations between CC and CP channels. A 'x' indicates the uncertainty is applied to that channel and thus correlated to the other channel with the same systematic. bhel0d + 0h + 0i dataset.

10 $Z\gamma$ Cross Section Measurement in Electron Channel

10.1 Previous measurement

The previous measurement with 200 pb^{-1} of data is shown in figure 7. This is a statistically limited measurement.

	Number of Events		
	$Z^0\gamma \to e^+e^-\gamma$		$Z^0\gamma \to \mu^+\mu^-\gamma$
	CC	CP	
$Z^0 + \gamma$	19.7 ± 0.8	11.4 ± 0.6	33.6 ± 1.5
$Z^0 + jet$	1.6 ± 0.5	1.2 ± 0.37	2.1 ± 0.7
total SM + BG	21.3 ± 0.9	12.6 ± 0.7	35.7 ± 1.7
Data	24	12	35

- $Z^0\gamma \to e^+e^-\gamma$ (CC) : $\sigma \times BR = 5.1 \pm 1.0(\text{stat}) \pm 0.2(\text{sys}) \pm 0.3(\text{lumi})$ pb
- $Z^0\gamma \to e^+e^-\gamma$ (CP) : $\sigma \times BR = 4.3 \pm 1.2(\text{stat}) \pm 0.3(\text{sys}) \pm 0.3(\text{lumi})$ pb
- $Z^0\gamma \to e^+e^-$: $\sigma \times BR = 4.8 \pm 0.8(\text{stat}) \pm 0.3(\text{sys}) \pm 0.3(\text{lumi})$ pb
- $Z^0\gamma \to \mu^+\mu^-\gamma$: $\sigma \times BR = 4.4 \pm 0.8(\text{stat}) \pm 0.2(\text{sys}) \pm 0.3(\text{lumi})$ pb

Figure 7: $Z\gamma$ cross section, cdf note 7996, 200pb^{-1}

10.2 Measure $Z\gamma$ Cross Section

The $Z\gamma$ cross section is calculated as:

$$\sigma_{ee\gamma} = \frac{N^{\text{obs}} - N^{\text{bkg}}}{A \cdot \epsilon \cdot \int \mathcal{L}dt}$$

where,

- N^{obs}: number of observed $Z\gamma$ Events
- N^{bkg}: number of background Events
- A: $Z\gamma$ acceptance
- ϵ: $Z\gamma$ event selection efficiency
- $\int \mathcal{L}dt$: integrated luminosity

10.3 $Z\gamma$ Acceptance x Efficiency Calculation

The $Z\gamma$ cross section will be quoted in a specific kinematic range. For example, for the ISR dominate sample, the cross section is quoted in the following kinematic range: E_T^{γ} >7 GeV, $\Delta R_{e\gamma}$ >0.7, M_{ee} >40 GeV/c^2 , $M_{ee\gamma}$ >100 GeV/c^2

The acceptance x efficiency is calculated as:

$$A \cdot \epsilon_{MC} = \frac{N_{ee\gamma}}{N_{gen}} \tag{10}$$

where,

- $N_{ee\gamma}$: number of events passing the $ee\gamma$ event selection criteria
- N_{gen}: number of events generated **in the above kinematic range**

The number of expected SM $ee\gamma$ events is determined as:

$$N_{SM}^{exp} = \sigma_{NLO} \cdot A \cdot \epsilon_{MC} \cdot SF \cdot \int \mathcal{L} dt \tag{11}$$

where,

- σ_{NLO}: NLO cross-section **in the above kinematic range**
- SF = $\frac{\epsilon_{Data}}{\epsilon MC}$

The measured cross-section **in the above kinematic range** is then simplified to:

$$\sigma_{ee\gamma} = \frac{N^{\text{obs}} - N^{\text{bkg}}}{A \cdot \epsilon \cdot \int \mathcal{L} dt} = \frac{N^{\text{obs}} - N^{\text{bkg}}}{N_{SM}^{exp}} \cdot \sigma_{NLO} \tag{12}$$

10.4 $Z\gamma$ Cross Section

The $Z\gamma$ cross sections using 1.07fb^{-1} of data are presented in Tables 11 - 13. The measurement for $M_{ee\gamma}$ < 100 GeV/c^2 , dominated by $Z \to ee\gamma$ final state radiation, is shown in Table 11. Table 12 is the cross section result for events with $M_{ee\gamma}$ > 100 GeV/c^2 and is predominately due to events with photon emission from initial state radiation. Finally Table 13 shows the total cross section for $p\bar{p} \to e^+e^-\gamma + X$ with E_T^{γ} > 7 GeV, $\Delta R_{e\gamma}$ > 0.7 and M_{ee} > 40 GeV/c^2 . We also have divided the data set into 3 parts(0d, 0h and 0i datasets) and measured the same three cross sections for each section of the data as described in Sections 10.4.1 - 10.4.3. The loose Z selection criteria doubles the $Z\gamma$ acceptance obtained in the previous measurement(Sec. 10.1).

Figure 8 compares the measured cross section to theory predictions.

10.4.1 $Z\gamma$ Cross Section – bhel0d dataset

The $Z\gamma$ cross sections for bhel0d dataset are shown in tables 14 - 16.

$\int \mathcal{L}dt(pb^{-1})$	1074		
$\sigma_{NLO}(pb)$	3.3±0.3		
$Z\gamma$ type	FSR		
Photon type	Central Photon		
Zee type	CC	CP	CC + CP
$N^{bkg}_{\gamma+Jet}$	0.3 ± 0.3	2.1 ± 1.3	2.4 ± 1.6
N^{bkg}_{Z+Jet}	3.7 ± 1.2	5.7 ± 2.0	9.4 ± 3.2
N^{exp}_{SM}	101.3 ± 5.5	107.1 ± 5.9	208.4 ± 11.1
$N^{exp}_{SM} + N^{bkg}_{QCD}$	105.3 ± 5.6	114.9 ± 6.3	220.2 ± 11.7
N^{obs}	129	107	236
σ^{obs}(pb)			
CC	4.1 ± 0.4 (stat.) ± 0.2 (syst.) ± 0.2 (lum.)		
CP	3.1 ± 0.3 (stat.) ± 0.2 (syst.) ± 0.2 (lum.)		
CC + CP	3.6 ± 0.2 (stat.) ± 0.2 (syst.) ± 0.2 (lum.)		

Table 11: Input parameters to the FSR $ee\gamma$ cross-section calculation, $1074pb^{-1}$. $E_T^{\gamma} > 7$ GeV, $\Delta R_{e\gamma} > 0.7$, $M_{ee} > 40$ GeV/c^2 and $M_{ee\gamma} < 100$ GeV/c^2 .

$\int \mathcal{L}dt(pb^{-1})$	1074		
$\sigma_{NLO}(pb)$	1.4±0.1		
$Z\gamma$ type	ISR		
Photon type	Central Photon		
Zee type	CC	CP	CC + CP
$N^{bkg}_{\gamma+Jet}$	1.5 ± 1.0	10.0 ± 4.5	11.5 ± 5.6
N^{bkg}_{Z+Jet}	7.8 ± 3.1	19.9 ± 7.9	27.8 ± 11.1
N^{exp}_{SM}	41.5 ± 2.2	75.7 ± 4.2	117.2 ± 6.3
$N^{exp}_{SM} + N^{bkg}_{QCD}$	50.9 ± 4.0	105.6 ± 10.1	156.4 ± 13.9
N^{obs}	54	100	154
σ^{obs}(pb)			
CC	1.5 ± 0.2 (stat.) ± 0.1 (syst.) ± 0.1 (lum.)		
CP	1.3 ± 0.2 (stat.) ± 0.2 (syst.) ± 0.1 (lum.)		
CC + CP	1.4 ± 0.1 (stat.) ± 0.2 (syst.) ± 0.1 (lum.)		

Table 12: Input parameters to the ISR $ee\gamma$ cross-section calculation, $1074pb^{-1}$. $E_T^{\gamma} > 7$ GeV, $\Delta R_{e\gamma} > 0.7$, $M_{ee} > 40$ GeV/c^2 and $M_{ee\gamma} > 100$ GeV/c^2 .

10.4.2 $Z\gamma$ Cross Section – bhel0h dataset

The $Z\gamma$ cross sections for bhel0h dataset are shown in tables 17 - 19.

$\int \mathcal{L}dt(pb^{-1})$	1074		
$\sigma_{NLO}(pb)$	4.7±0.4		
$Z\gamma$ type	FSR+ISR		
Photon type	Central Photon		
Zee type	CC	CP	CC + CP
$N^{bkg}_{\gamma+Jet}$	1.8 ± 1.2	12.1 ± 5.4	13.9 ± 6.5
N^{bkg}_{Z+Jet}	11.5 ± 4.3	25.6 ± 9.9	37.1 ± 14.3
N^{exp}_{SM}	142.6 ± 7.7	181.2 ± 10.0	323.8 ± 17.3
$N^{exp}_{SM} + N^{bkg}_{QCD}$	155.9 ± 8.9	218.9 ± 15.1	374.8 ± 23.4
N^{obs}	183	207	390
σ^{obs}(pb)			
CC	5.6 ± 0.4 (stat.) ± 0.3 (syst.) ± 0.3 (lum.)		
CP	4.4 ± 0.4 (stat.) ± 0.4 (syst.) ± 0.3 (lum.)		
CC + CP	4.9 ± 0.3 (stat.) ± 0.3 (syst.) ± 0.3 (lum.)		

Table 13: Input parameters to the FSR+ISR $ee\gamma$ cross-section calculation, $1074pb^{-1}$. $E_T^\gamma > 7$ GeV, $\Delta R_{e\gamma} > 0.7$ and $M_{ee} > 40$ GeV/c^2 .

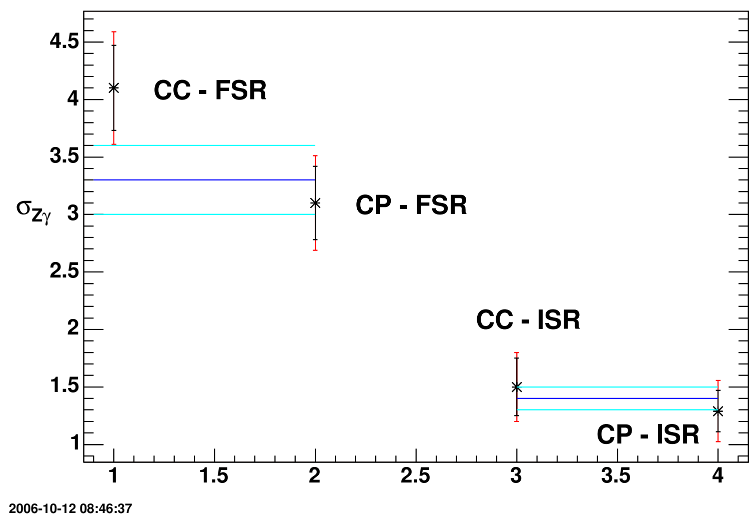

Figure 8: Compare σ^{obs} to theory prediction. The uncertainty in σ^{obs} includes stat., syst. and luminosity uncertainties, stat only uncercertainty is shown in black. Theory predictions are shown in blue with uncertainty bands. 4 independent measurements, 3 of them are within 1 sigma.

$\int \mathcal{L}dt(pb^{-1})$	372.7		
$\sigma_{NLO}(pb)$	3.3±0.3		
$Z\gamma$ type	FSR		
Photon type	Central Photon		
Zee type	CC	CP	CC + CP
SF	0.96	0.94	
$A \cdot \epsilon_{MC} \cdot SF$	2.9 %	3.1 %	6.0 %
$N^{bkg}_{\gamma+Jet}$	0.1 ± 0.1	0.4 ± 0.3	0.5 ± 0.4
N^{bkg}_{Z+Jet}	1.1 ± 0.4	1.9 ± 0.7	2.9 ± 1.0
N^{exp}_{SM}	36.1 ± 2.0	37.8 ± 2.1	73.8 ± 3.9
$N^{exp}_{SM} + N^{bkg}_{QCD}$	37.2 ± 2.0	40.0 ± 2.2	77.3 ± 4.1
N^{obs}	44	30	74
σ^{obs}(pb)			
CC	3.9 ± 0.6 (stat.) ± 0.2 (syst.) ± 0.2 (lum.)		
CP	2.4 ± 0.5 (stat.) ± 0.1 (syst.) ± 0.1 (lum.)		
CC + CP	3.2 ± 0.4 (stat.) ± 0.2 (syst.) ± 0.2 (lum.)		

Table 14: Input parameters to the FSR $ee\gamma$ cross-section calculation, bhel0d dataset, $372pb^{-1}$. $E_T^{\gamma} > 7$ GeV, $\Delta R_{e\gamma} > 0.7$, $M_{ee} > 40$ GeV/c^2 and $M_{ee\gamma} < 100$ GeV/c^2 .

$\int \mathcal{L}dt(pb^{-1})$	372.7		
$\sigma_{NLO}(pb)$	1.4±0.1		
$Z\gamma$ type	ISR		
Photon type	Central Photon		
Zee type	CC	CP	CC + CP
SF	0.96	0.94	
$A \cdot \epsilon_{MC} \cdot SF$	2.8 %	5.2 %	8.0 %
$N^{bkg}_{\gamma+Jet}$	0.2 ± 0.2	2.1 ± 1.0	2.3 ± 1.2
N^{bkg}_{Z+Jet}	2.6 ± 1.0	6.4 ± 2.6	9.0 ± 3.6
N^{exp}_{SM}	14.7 ± 0.8	27.1 ± 1.5	41.8 ± 2.2
$N^{exp}_{SM} + N^{bkg}_{QCD}$	17.5 ± 1.3	35.7 ± 3.2	53.1 ± 4.4
N^{obs}	21	41	62
σ^{obs}(pb)			
CC	1.7 ± 0.4 (stat.) ± 0.1 (syst.) ± 0.1 (lum.)		
CP	1.7 ± 0.3 (stat.) ± 0.2 (syst.) ± 0.1 (lum.)		
CC + CP	1.7 ± 0.3 (stat.) ± 0.2 (syst.) ± 0.1 (lum.)		

Table 15: Input parameters to the ISR $ee\gamma$ cross-section calculation, bhel0d dataset, $372pb^{-1}$. $E_T^{\gamma} > 7$ GeV, $\Delta R_{e\gamma} > 0.7$, $M_{ee} > 40$ GeV/c^2 and $M_{ee\gamma} > 100$ GeV/c^2 .

$\int \mathcal{L}dt(pb^{-1})$	372.7		
$\sigma_{NLO}(pb)$	4.7±0.4		
$Z\gamma$ type	FSR+ISR		
Photon type	Central Photon		
Zee type	CC	CP	CC + CP
SF	0.96	0.94	
$A \cdot \epsilon_{MC} \cdot SF$	2.9 %	3.6 %	6.5 %
$N^{bkg}_{\gamma+Jet}$	0.3 ± 0.2	2.5 ± 1.2	2.8 ± 1.4
N^{bkg}_{Z+Jet}	3.6 ± 1.4	8.3 ± 3.3	11.9 ± 4.6
N^{exp}_{SM}	50.5 ± 2.7	64.0 ± 3.5	114.5 ± 6.1
$N^{exp}_{SM} + N^{bkg}_{QCD}$	54.5 ± 3.1	74.8 ± 4.9	129.3 ± 7.8
N^{obs}	65	71	136
σ^{obs}(pb)			
CC	5.7 ± 0.8 (stat.) ± 0.3 (syst.) ± 0.3 (lum.)		
CP	4.4 ± 0.6 (stat.) ± 0.4 (syst.) ± 0.3 (lum.)		
CC + CP	5.0 ± 0.5 (stat.) ± 0.3 (syst.) ± 0.3 (lum.)		

Table 16: Input parameters to the FSR+ISR $ee\gamma$ cross-section calculation, bhel0d dataset, $372pb^{-1}$. $E_T^\gamma > 7$ GeV, $\Delta R_{e\gamma} > 0.7$ and $M_{ee} > 40$ GeV/c^2 .

$\int \mathcal{L}dt(pb^{-1})$	428		
$\sigma_{NLO}(pb)$	3.3±0.3		
$Z\gamma$ type	FSR		
Photon type	Central Photon		
Zee type	CC	CP	CC + CP
SF	0.93	0.92	
$A \cdot \epsilon_{MC} \cdot SF$	2.8 %	3.0 %	5.8 %
$N^{bkg}_{\gamma+Jet}$	0.0 ± 0.0	1.0 ± 0.6	1.0 ± 0.6
N^{bkg}_{Z+Jet}	1.6 ± 0.5	2.4 ± 0.8	4.0 ± 1.3
N^{exp}_{SM}	39.8 ± 2.2	42.8 ± 2.4	82.6 ± 4.4
$N^{exp}_{SM} + N^{bkg}_{QCD}$	41.4 ± 2.2	46.2 ± 2.6	87.6 ± 4.6
N^{obs}	59	50	109
σ^{obs}(pb)			
CC	4.8 ± 0.6 (stat.) ± 0.3 (syst.) ± 0.3 (lum.)		
CP	3.6 ± 0.5 (stat.) ± 0.2 (syst.) ± 0.2 (lum.)		
CC + CP	4.2 ± 0.4 (stat.) ± 0.2 (syst.) ± 0.2 (lum.)		

Table 17: Input parameters to the FSR $ee\gamma$ cross-section calculation, bhel0h dataset, $428pb^{-1}$. $E_T^\gamma > 7$ GeV, $\Delta R_{e\gamma} > 0.7$, $M_{ee} > 40$ GeV/c^2 and $M_{ee\gamma} < 100$ GeV/c^2 .

$\int \mathcal{L}dt(pb^{-1})$	428		
$\sigma_{NLO}(pb)$	1.4±0.1		
$Z\gamma$ type	ISR		
Photon type	Central Photon		
Zee type	CC	CP	CC + CP
SF	0.93	0.92	
$A \cdot \epsilon_{MC} \cdot SF$	2.8 %	5.0 %	7.8 %
$N^{bkg}_{\gamma+Jet}$	0.6 ± 0.4	3.8 ± 1.7	4.3 ± 2.0
N^{bkg}_{Z+Jet}	3.1 ± 1.3	8.0 ± 3.2	11.1 ± 4.5
N^{exp}_{SM}	16.6 ± 0.9	29.9 ± 1.6	46.5 ± 2.5
$N^{exp}_{SM} + N^{bkg}_{QCD}$	20.3 ± 1.6	41.7 ± 4.0	61.9 ± 5.5
N^{obs}	19	31	50
σ^{obs}(pb)			
CC	1.3 ± 0.4 (stat.) ± 0.1 (syst.) ± 0.1 (lum.)		
CP	0.9 ± 0.3 (stat.) ± 0.2 (syst.) ± 0.1 (lum.)		
CC + CP	1.0 ± 0.2 (stat.) ± 0.2 (syst.) ± 0.1 (lum.)		

Table 18: Input parameters to the ISR $ee\gamma$ cross-section calculation, bhel0h dataset, $428pb^{-1}$. $E_T^\gamma > 7$ GeV, $\Delta R_{e\gamma} > 0.7$, $M_{ee} > 40$ GeV/c^2 and $M_{ee\gamma} > 100$ GeV/c^2 .

$\int \mathcal{L}dt(pb^{-1})$	428		
$\sigma_{NLO}(pb)$	4.7±0.4		
$Z\gamma$ type	FSR+ISR		
Photon type	Central Photon		
Zee type	CC	CP	CC + CP
SF	0.93	0.92	
$A \cdot \epsilon_{MC} \cdot SF$	2.8 %	3.6 %	6.4 %
$N^{bkg}_{\gamma+Jet}$	0.6 ± 0.4	4.8 ± 2.1	5.4 ± 2.4
N^{bkg}_{Z+Jet}	4.7 ± 1.8	10.4 ± 4.0	15.1 ± 5.8
N^{exp}_{SM}	56.4 ± 3.1	72.3 ± 4.0	128.7 ± 6.9
$N^{exp}_{SM} + N^{bkg}_{QCD}$	61.7 ± 3.5	87.4 ± 6.0	149.1 ± 9.3
N^{obs}	78	81	159
σ^{obs}(pb)			
CC	6.1 ± 0.7 (stat.) ± 0.4 (syst.) ± 0.4 (lum.)		
CP	4.3 ± 0.6 (stat.) ± 0.4 (syst.) ± 0.2 (lum.)		
CC + CP	5.1 ± 0.5 (stat.) ± 0.4 (syst.) ± 0.3 (lum.)		

Table 19: Input parameters to the FSR+ISR $ee\gamma$ cross-section calculation, bhel0h dataset, $428pb^{-1}$. $E_T^\gamma > 7$ GeV, $\Delta R_{e\gamma} > 0.7$ and $M_{ee} > 40$ GeV/c^2 .

10.4.3 $Z\gamma$ Cross Section – bhel0i dataset

The $Z\gamma$ cross sections for bhel0i dataset are shown in tables 20 - 22.

$\int \mathcal{L}dt(pb^{-1})$	273.5		
$\sigma_{NLO}(pb)$	3.3±0.3		
$Z\gamma$ type	FSR		
Photon type	Central Photon		
Zee type	CC	CP	CC + CP
SF	0.93	0.92	
$A \cdot \epsilon_{MC} \cdot SF$	2.8 %	2.9 %	5.8 %
$N^{bkg}_{\gamma+Jet}$	0.2 ± 0.2	0.6 ± 0.4	0.8 ± 0.6
N^{bkg}_{Z+Jet}	1.0 ± 0.3	1.5 ± 0.5	2.5 ± 0.8
N^{exp}_{SM}	25.4 ± 1.4	26.6 ± 1.5	52.0 ± 2.8
$N^{exp}_{SM} + N^{bkg}_{QCD}$	26.6 ± 1.4	28.6 ± 1.6	55.3 ± 3.0
N^{obs}	26	27	53
σ^{obs}(pb)			
CC	3.2 ± 0.7 (stat.) ± 0.2 (syst.) ± 0.2 (lum.)		
CP	3.1 ± 0.6 (stat.) ± 0.2 (syst.) ± 0.2 (lum.)		
CC + CP	3.2 ± 0.5 (stat.) ± 0.2 (syst.) ± 0.2 (lum.)		

Table 20: Input parameters to the FSR $ee\gamma$ cross-section calculation, bhel0i dataset, $273pb^{-1}$. $E_T^{\gamma} > 7$ GeV, $\Delta R_{e\gamma} > 0.7$, $M_{ee} > 40$ GeV/c^2 and $M_{ee\gamma} < 100$ GeV/c^2 .

$\int \mathcal{L}dt(pb^{-1})$	273.5		
$\sigma_{NLO}(pb)$	1.4±0.1		
$Z\gamma$ type	ISR		
Photon type	Central Photon		
Zee type	CC	CP	CC + CP
SF	0.93	0.92	
$A \cdot \epsilon_{MC} \cdot SF$	2.7 %	4.9 %	7.6 %
$N^{bkg}_{\gamma+Jet}$	0.8 ± 0.5	4.1 ± 1.9	4.9 ± 2.4
N^{bkg}_{Z+Jet}	2.2 ± 0.8	5.5 ± 2.1	7.6 ± 3.0
N^{exp}_{SM}	10.2 ± 0.6	18.6 ± 1.0	28.9 ± 1.5
$N^{exp}_{SM} + N^{bkg}_{QCD}$	13.1 ± 1.1	28.2 ± 3.0	41.4 ± 4.1
N^{obs}	14	28	42
σ^{obs}(pb)			
CC	1.5 ± 0.5 (stat.) ± 0.2 (syst.) ± 0.1 (lum.)		
CP	1.4 ± 0.4 (stat.) ± 0.2 (syst.) ± 0.1 (lum.)		
CC + CP	1.4 ± 0.3 (stat.) ± 0.2 (syst.) ± 0.1 (lum.)		

Table 21: Input parameters to the ISR $ee\gamma$ cross-section calculation, bhel0i dataset, $273pb^{-1}$. $E_T^{\gamma} > 7$ GeV, $\Delta R_{e\gamma} > 0.7$, $M_{ee} > 40$ GeV/c^2 and $M_{ee\gamma} > 100$ GeV/c^2 .

$\int \mathcal{L}dt(pb^{-1})$	273.5		
$\sigma_{NLO}(pb)$	4.7±0.4		
$Z\gamma$ type	FSR+ISR		
Photon type	Central Photon		
Zee type	CC	CP	CC + CP
SF	0.93	0.92	
$A \cdot \epsilon_{MC} \cdot SF$	2.8 %	3.5 %	6.3 %
$N^{bkg}_{\gamma+Jet}$	1.0 ± 0.6	4.7 ± 2.1	5.7 ± 2.7
N^{bkg}_{Z+Jet}	3.2 ± 1.2	6.9 ± 2.6	10.1 ± 3.8
N^{exp}_{SM}	35.7 ± 1.9	45.0 ± 2.5	80.6 ± 4.3
$N^{exp}_{SM} + N^{bkg}_{QCD}$	39.8 ± 2.3	56.6 ± 4.2	96.4 ± 6.4
N^{obs}	40	55	95
σ^{obs}(pb)			
CC	4.7 ± 0.8 (stat.) ± 0.3 (syst.) ± 0.3 (lum.)		
CP	4.5 ± 0.8 (stat.) ± 0.4 (syst.) ± 0.3 (lum.)		
CC + CP	4.6 ± 0.6 (stat.) ± 0.4 (syst.) ± 0.3 (lum.)		

Table 22: Input parameters to the FSR+ISR $ee\gamma$ cross-section calculation, bhel0i dataset, $273pb^{-1}$. $E_T^{\gamma} > 7$ GeV, $\Delta R_{e\gamma} > 0.7$ and $M_{ee} > 40$ GeV/c^2 .

10.5 $Z\gamma$ Event Kinematics

The $Z\gamma$ event kinematics distribution plots are shown in figures 9 - 35. The kinematic distributions are compared to the SM predictions. There is generally good agreement with the SM predictions.

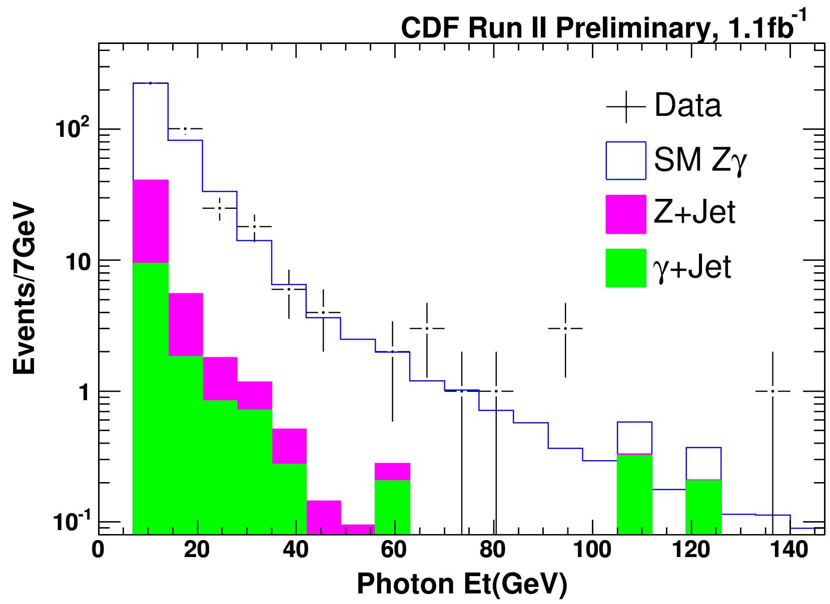

Figure 9: Photon Et Distribution, CC + CP , bhel0d, 0h and 0i datasets, 7 GeV photon Et cut.

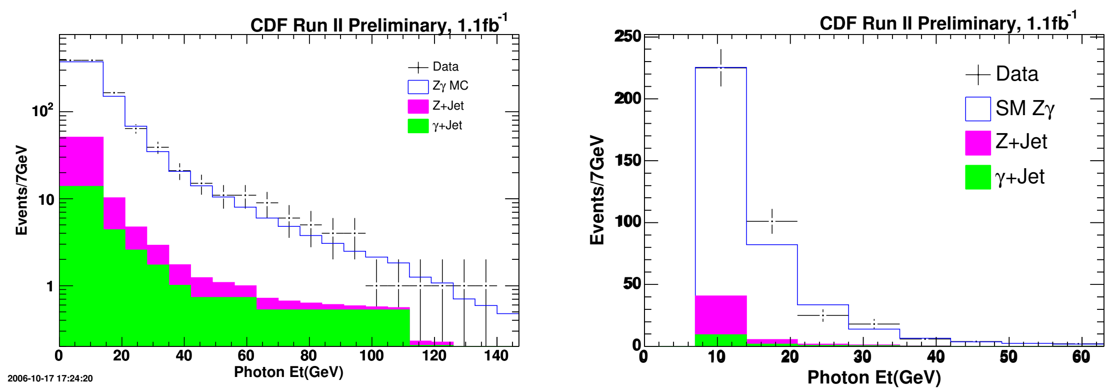

Figure 10: Photon Et Distribution, integral plot(left) , CC + CP , bhel0d, 0h and 0i datasets, 7 GeV photon Et cut.

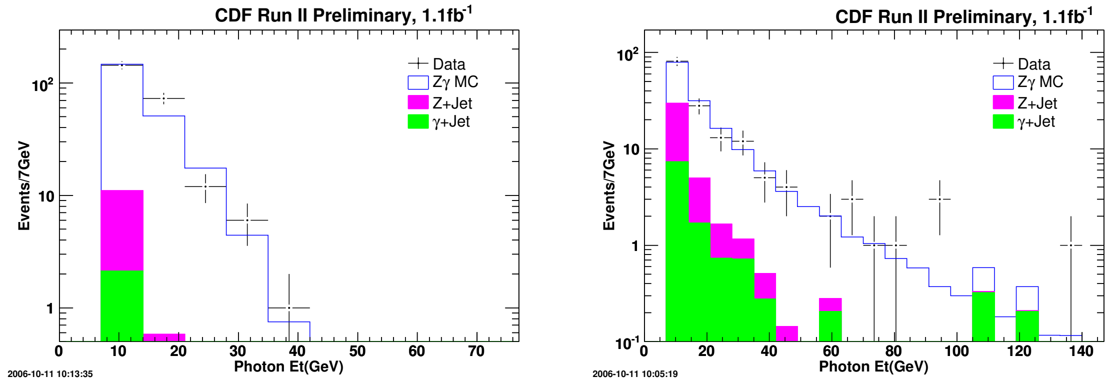

Figure 11: Photon Et Distribution, CC + CP , bhel0d, 0h and 0i datasets, 7 GeV photon Et cut. FSR(left), ISR(right).

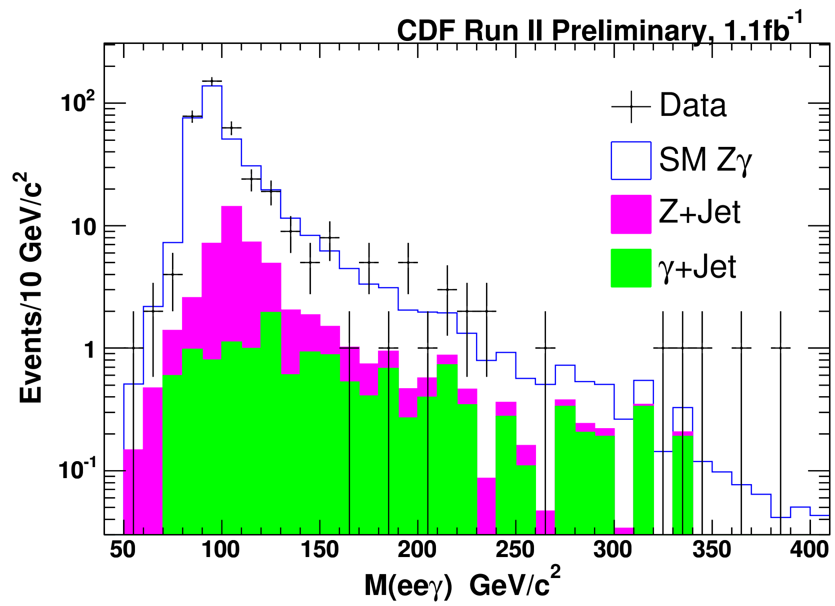

Figure 12: $M_{ee\gamma}$ Distribution, CC + CP , 1fb^{-1}, 7 GeV photon Et cut.

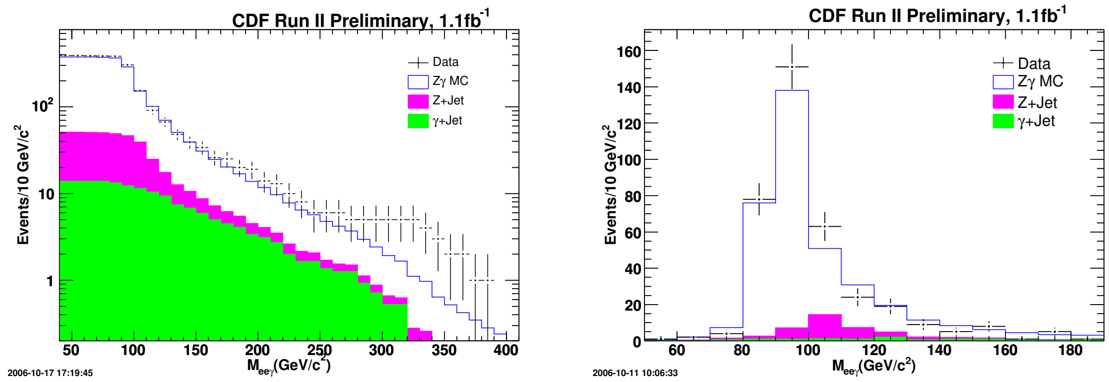

Figure 13: $M_{ee\gamma}$ Distribution, integral plot(left), CC + CP , 1fb^{-1}, 7 GeV photon Et cut.

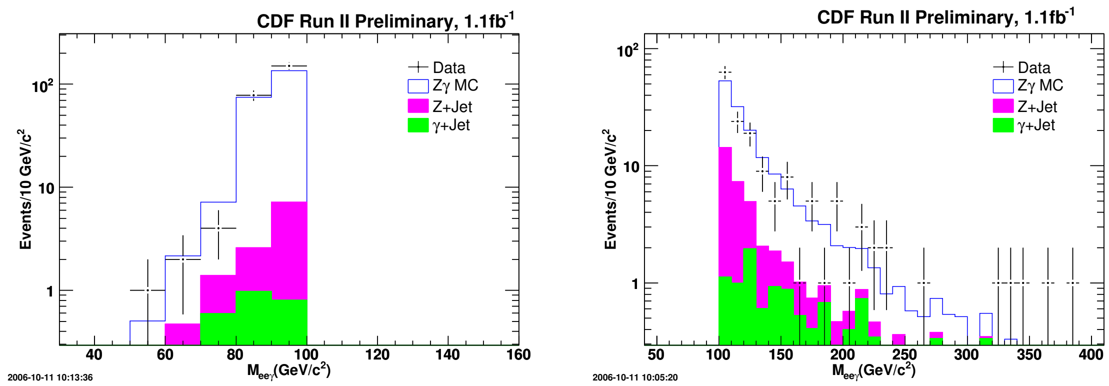

Figure 14: $M_{ee\gamma}$ Distribution, CC + CP , 1fb^{-1}, 7 GeV photon Et cut. FSR(left), ISR(right).

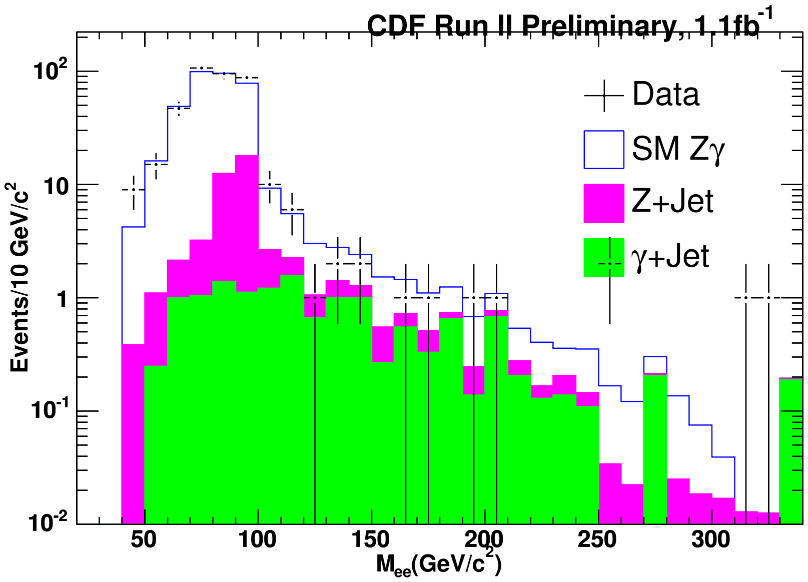

Figure 15: M_{ee} Distribution, CC + CP , 1fb^{-1}, 7 GeV photon Et cut.

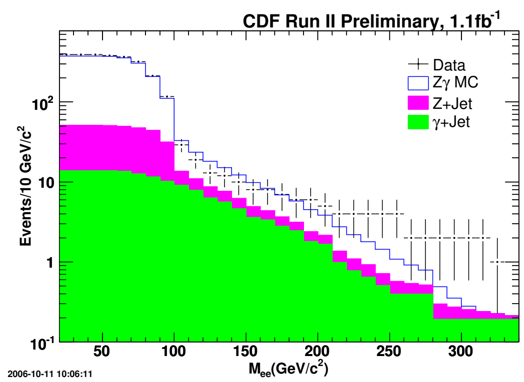

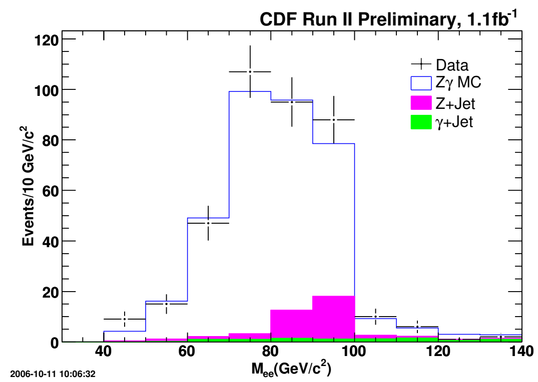

Figure 16: M_{ee} Distribution, integral plot(left), CC + CP , 1fb^{-1}, 7 GeV photon Et cut.

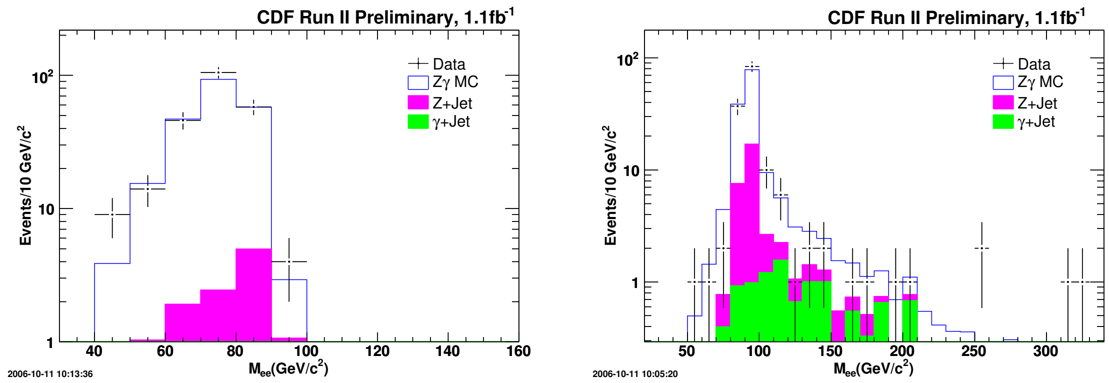

Figure 17: M_{ee} Distribution, CC + CP , 1fb^{-1}, 7 GeV photon Et cut. FSR(left), ISR(right).

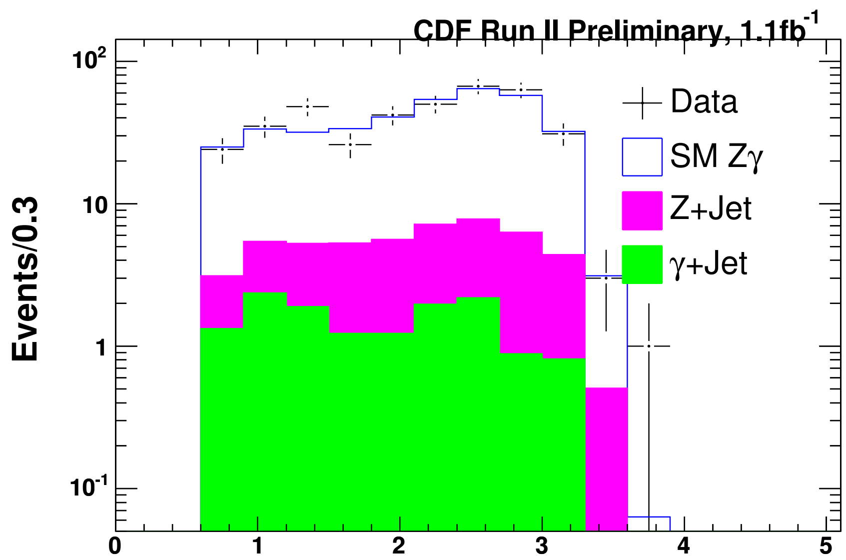

Figure 18: DeltaRb Distribution, CC + CP , 1fb^{-1}, 7 GeV photon Et cut.

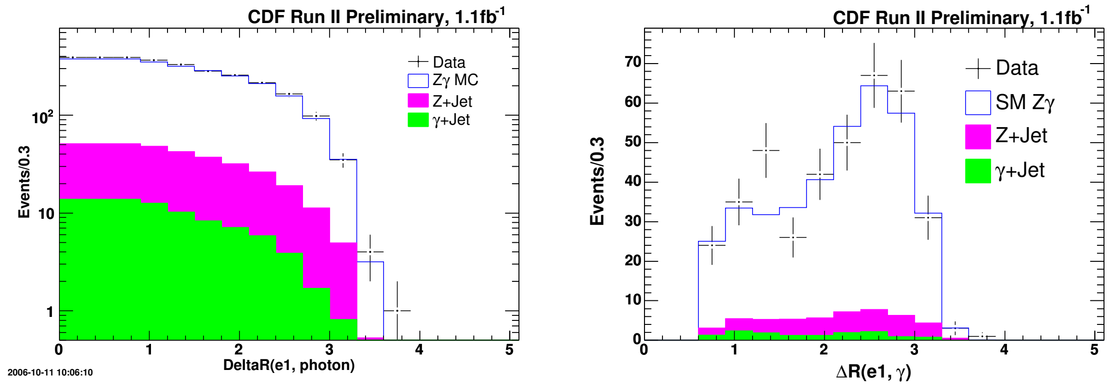

Figure 19: DeltaRa Distribution, integral plot(left), CC + CP , 1fb^{-1}, 7 GeV photon Et cut.

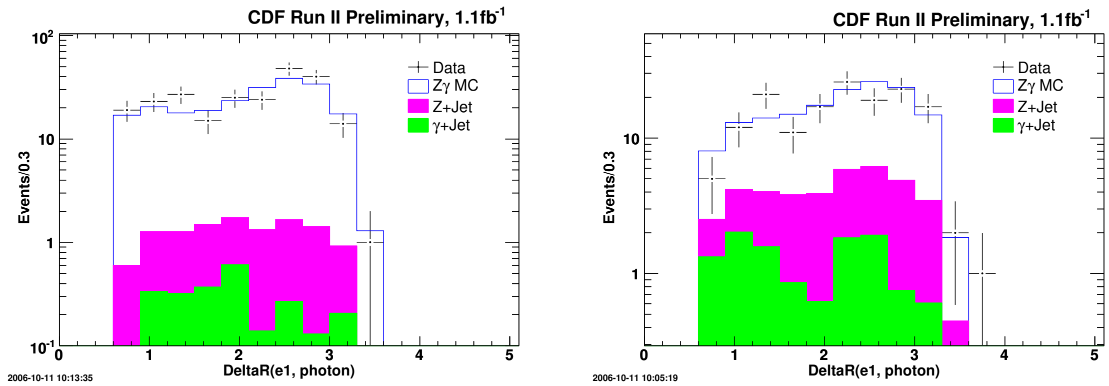

Figure 20: DeltaRa Distribution, CC + CP , 1fb^{-1}, 7 GeV photon Et cut. FSR(left), ISR(right).

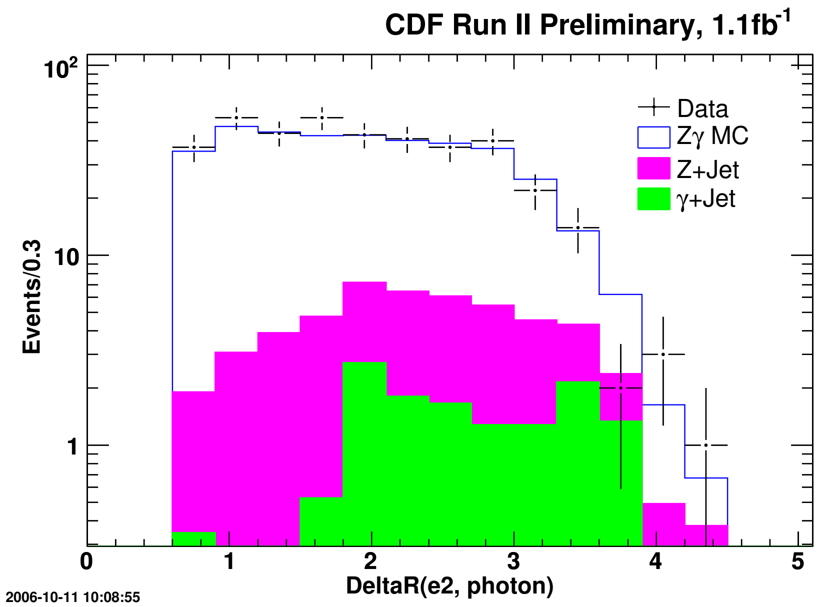

Figure 21: DeltaRb Distribution, CC + CP , 1fb^{-1}, 7 GeV photon Et cut.

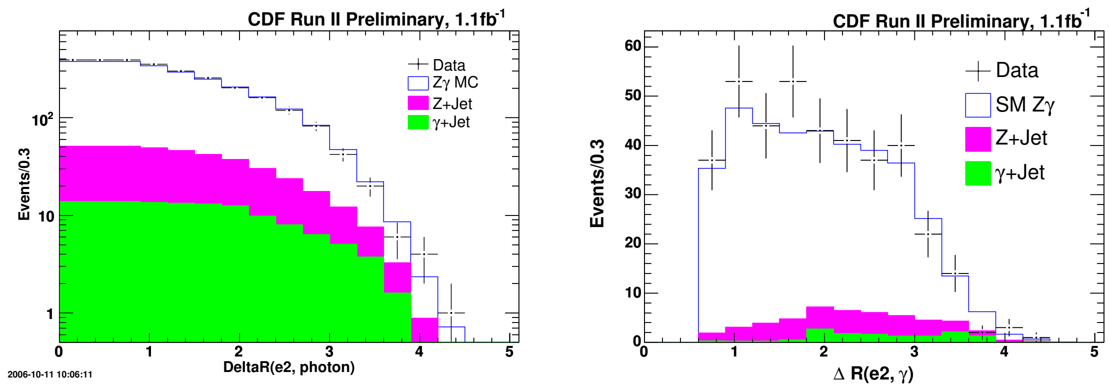

Figure 22: DeltaRb Distribution, integral plot(left), CC + CP , 1fb^{-1}, 7 GeV photon Et cut.

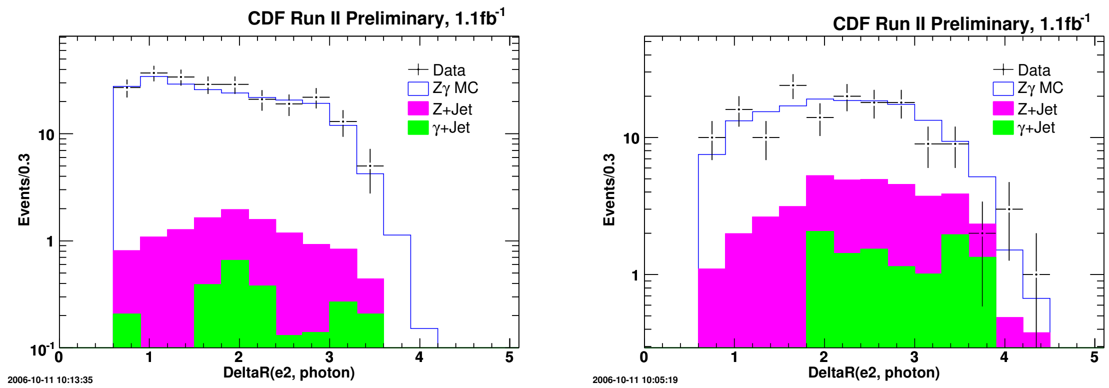

Figure 23: DeltaRb Distribution, CC + CP , 1fb^{-1}, 7 GeV photon Et cut. FSR(left), ISR(right).

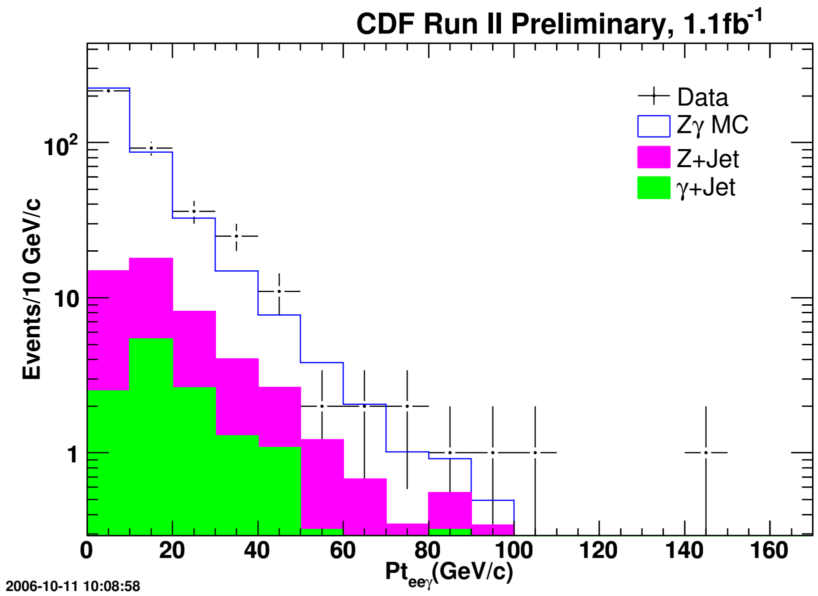

Figure 24: $P_T^{ee\gamma}$ Distribution, CC + CP , 1fb^{-1}, 7 GeV photon Et cut.

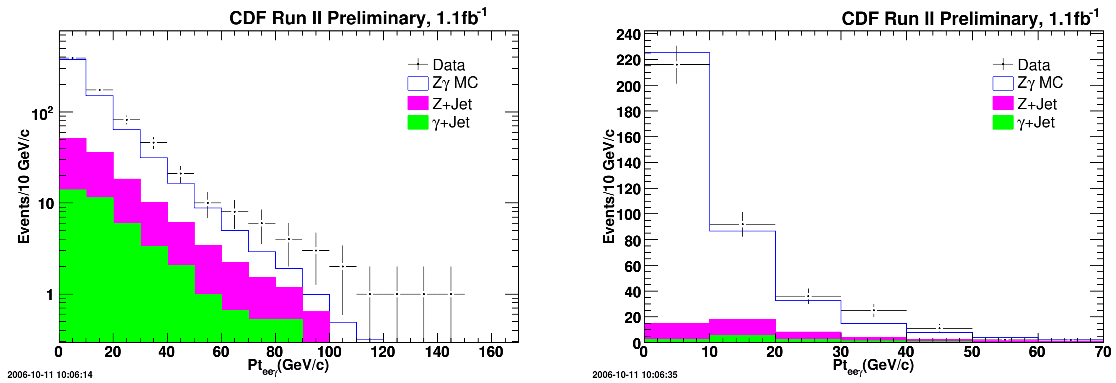

Figure 25: $P_T^{ee\gamma}$ Distribution, integral plot(left), CC + CP , 1fb^{-1}, 7 GeV photon Et cut.

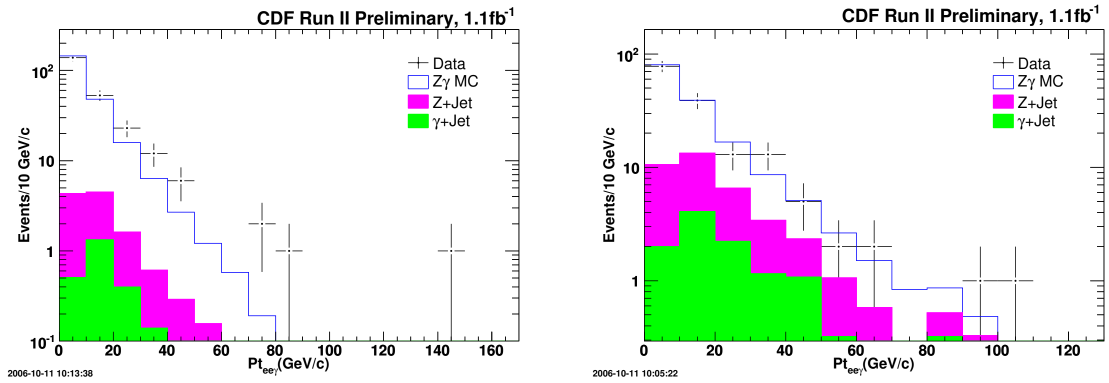

Figure 26: $P_T^{ee\gamma}$ Distribution, CC + CP , 1fb^{-1}, 7 GeV photon Et cut. FSR(left), ISR(right).

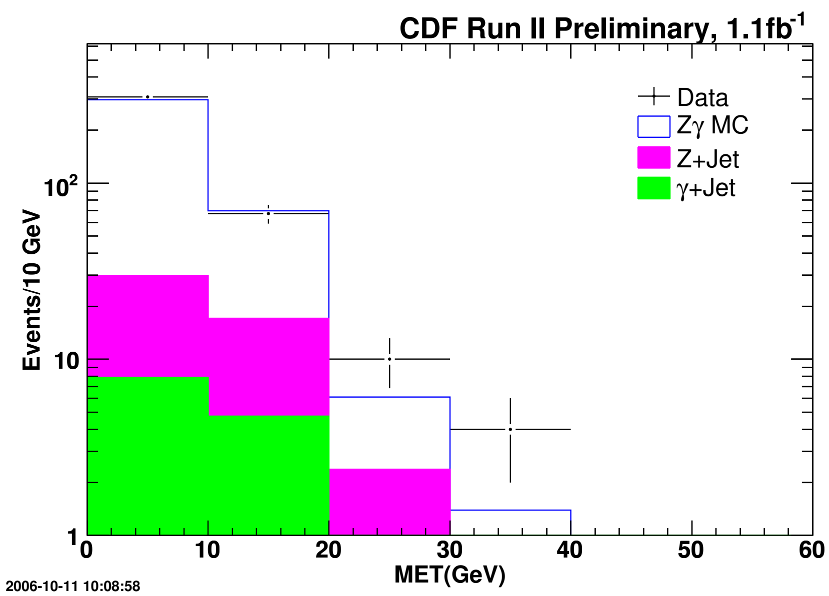

Figure 27: $\not\!\!E_T$ Distribution, CC + CP , 1fb^{-1}, 7 GeV photon Et cut.

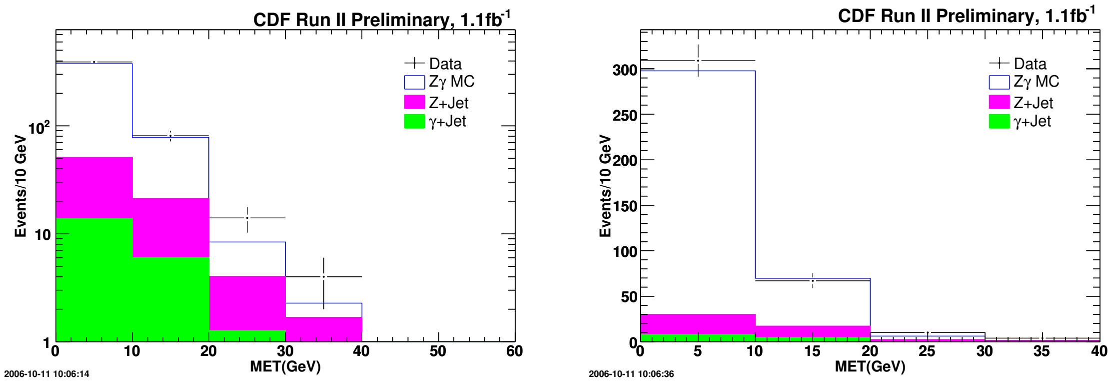

Figure 28: $\not\!\!E_T$ Distribution, integral plot(left), CC + CP , 1fb^{-1}, 7 GeV photon Et cut.

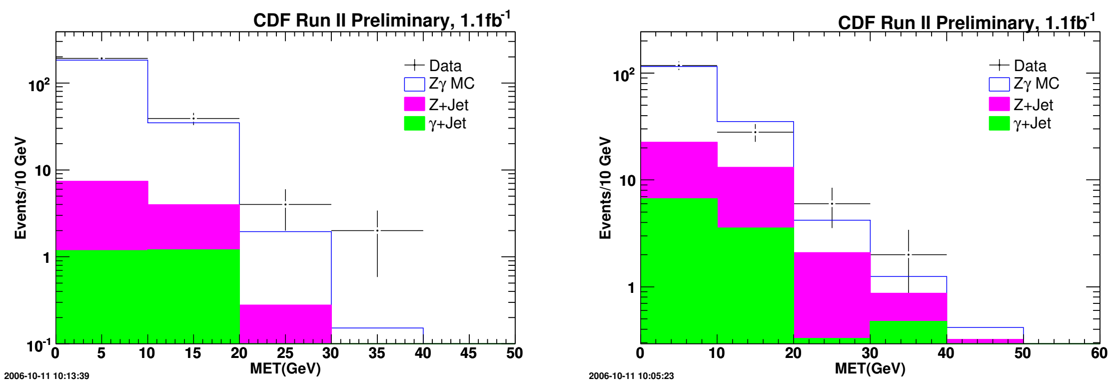

Figure 29: $\not\!\!E_T$ Distribution, CC + CP , 1fb^{-1}, 7 GeV photon Et cut. FSR(left), ISR(right).

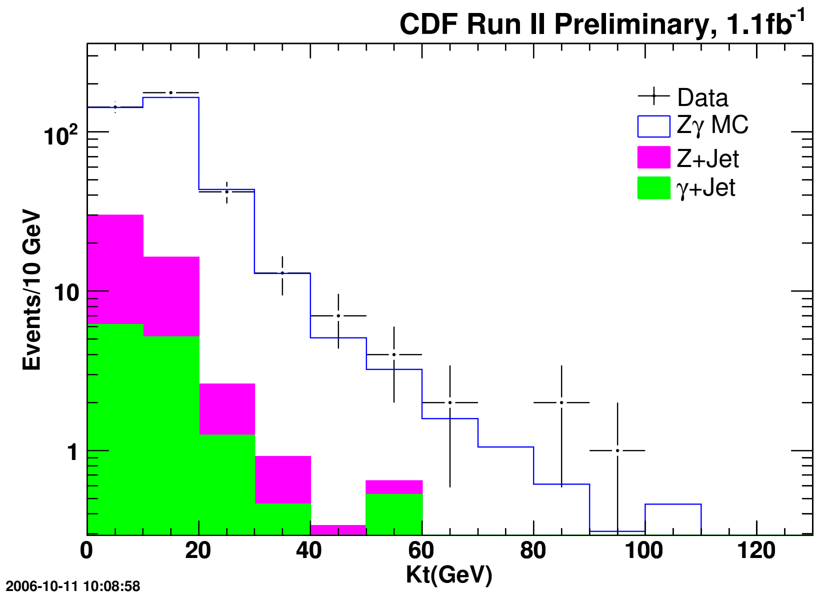

Figure 30: Kt Distribution, CC + CP , 1fb^{-1}, 7 GeV photon Et cut.

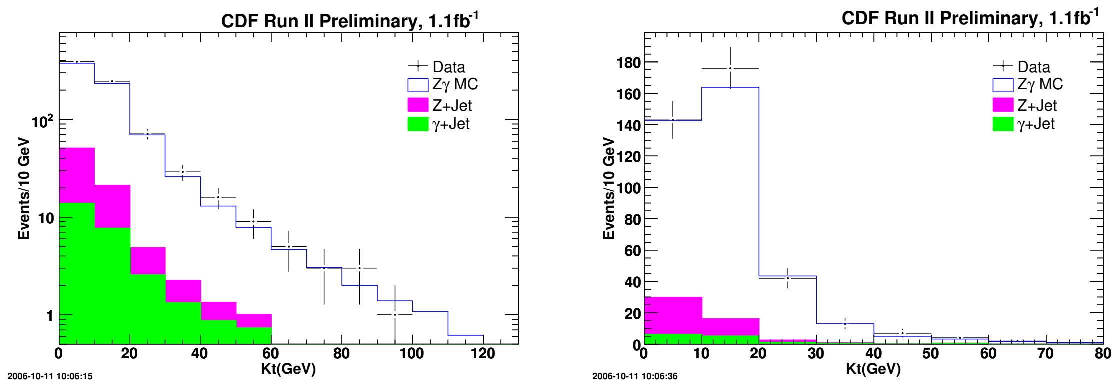

Figure 31: Kt Distribution, integral plot(left), CC + CP , 1fb^{-1}, 7 GeV photon Et cut.

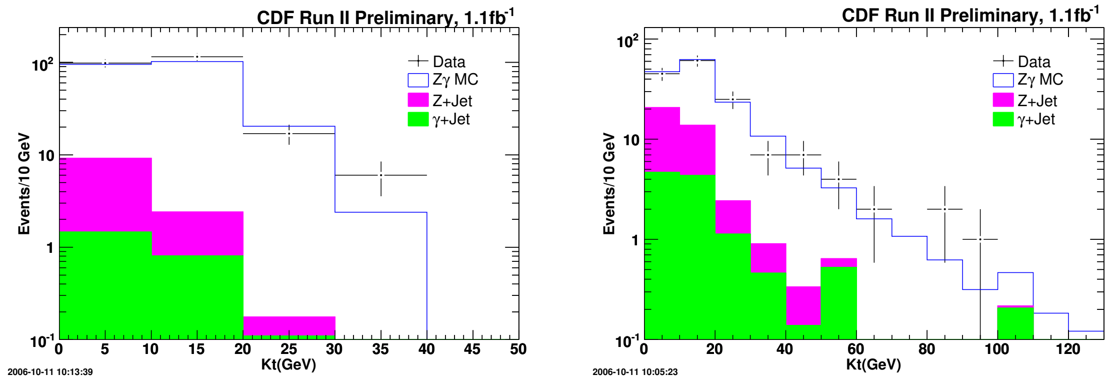

Figure 32: Kt Distribution, CC + CP , 1fb^{-1}, 7 GeV photon Et cut. FSR(left), ISR(right).

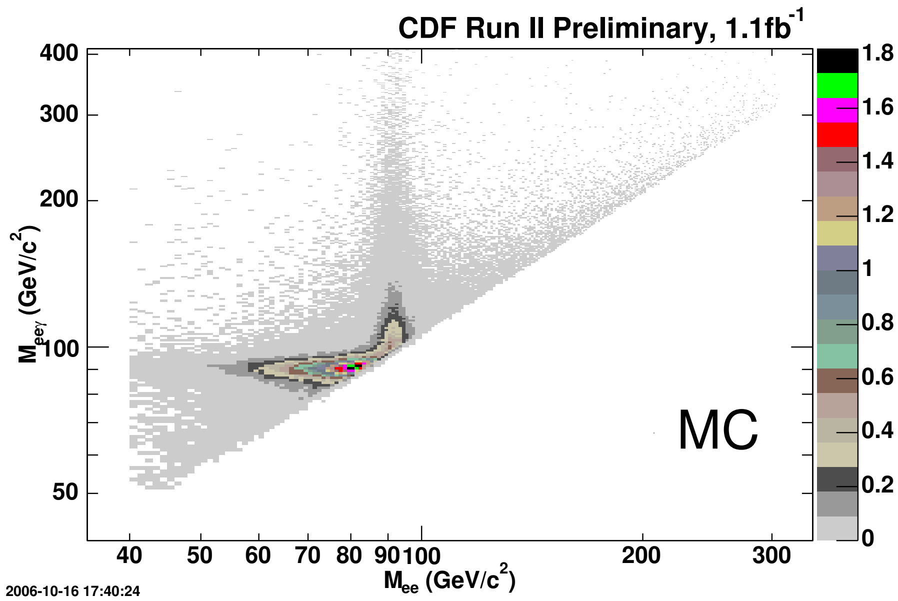

Figure 33: MC M_{ee} -$M_{ee\gamma}$ Distribution, CC + CP , 1fb^{-1}, 7 GeV photon Et cut.

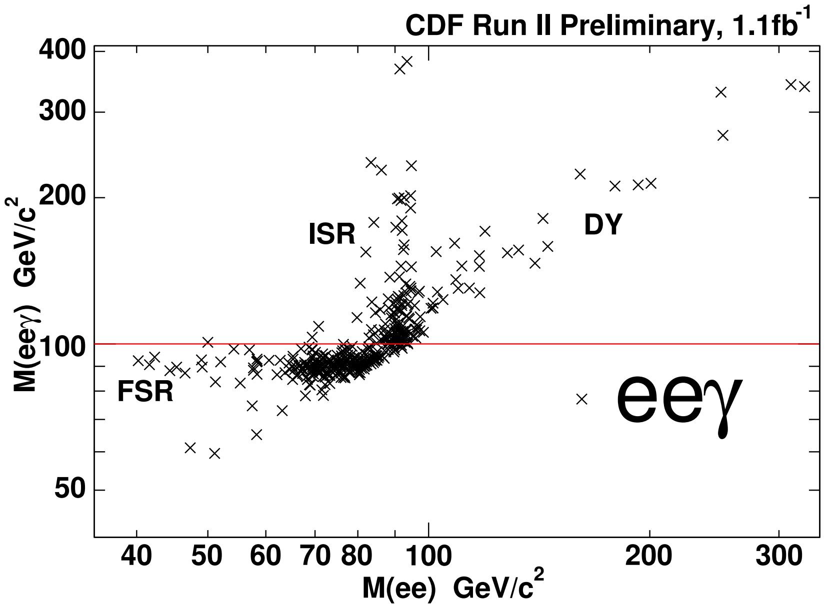

Figure 34: Data M_{ee} -$M_{ee\gamma}$ Distribution, CC + CP , 1fb^{-1}, 7 GeV photon Et cut.

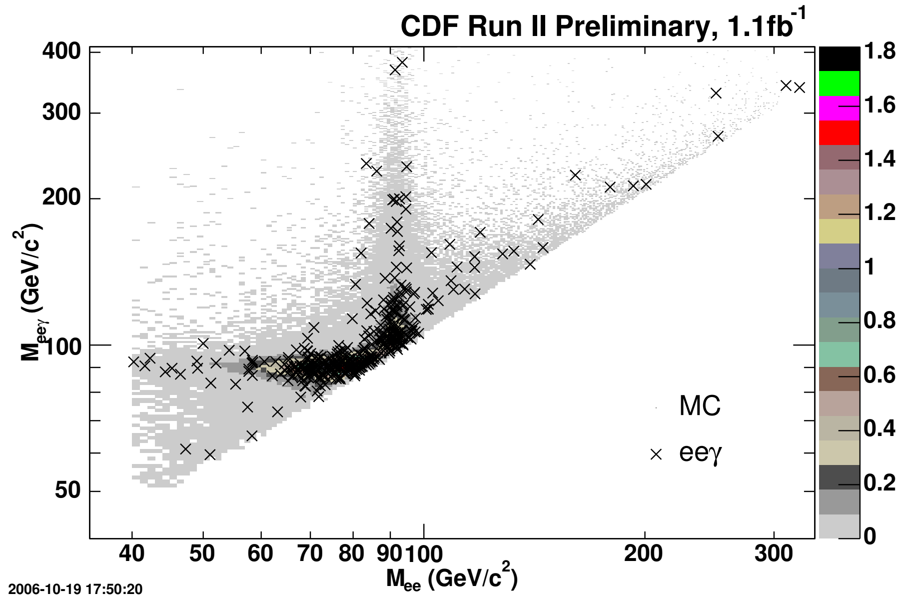

Figure 35: M_{ee} -$M_{ee\gamma}$ Distribution, CC + CP , 1fb^{-1}, 7 GeV photon Et cut.

10.6 $Z\gamma$ Event Display

In this section, a few events with very high M_{ee} , $M_{ee\gamma}$ and photon Et are displayed.

10.6.1 The Highest Photon E_T Event

Event 69435 in run 161830 has the highest photon E_T (=135GeV).

The kinematic of this event is as following:

Run	Event	Z Type	E_T^γ	$M_{ee\gamma}$	M_{ee}	$P_T^{ee\gamma}$	E_T^{e1}	E_T^{e2}	η^γ	η^{e1}	η^{e2}
161830	69435	CC	135	368	92	17	137	27	-0.6	0.8	-0.2

Table 23: The highest E_T^γ $Z\gamma$ event

Figure 36 and 37 show the COT view and calorimeter tower view of this event.

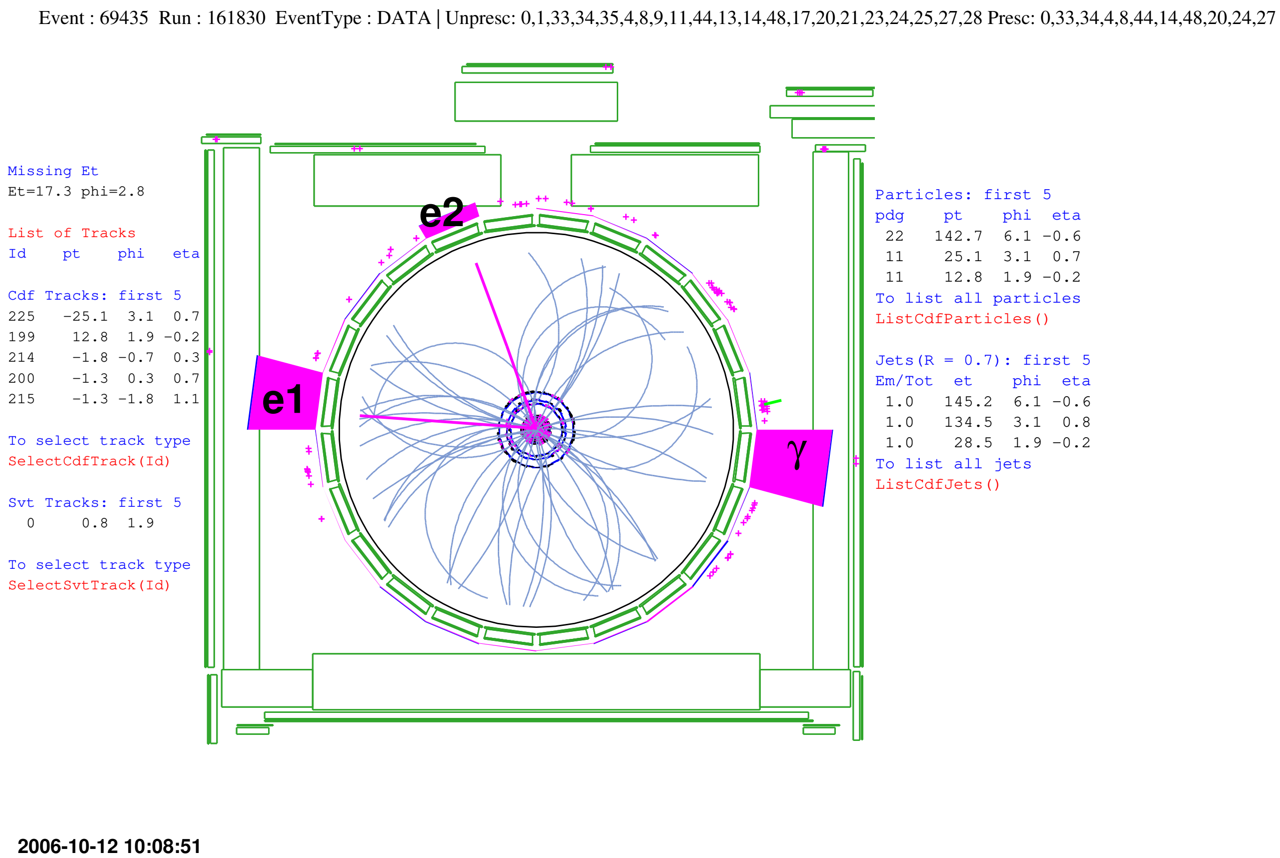

Figure 36: The COT view of the highest photon E_T event, event 69435 in run 161830.

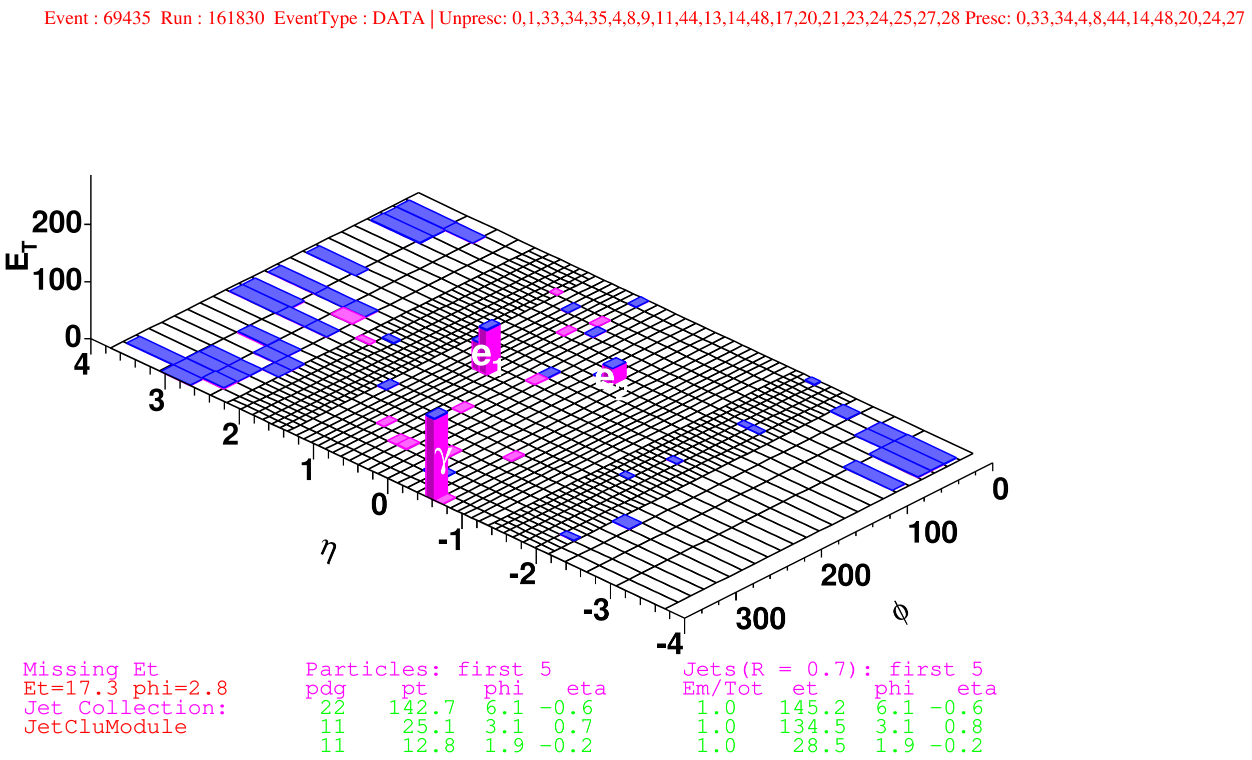

Figure 37: The calorimeter tower view of the highest photon E_T event, event 69435 in run 161830. Tower Et > 0.5 GeV.

10.6.2 The Highest $M_{ee\gamma}$ Event

Event 619905 in run 161555 has the highest $M_{ee\gamma}$ (=381GeV/c^2).

The kinematic of this event is as following:

Run	Event	Z Type	E_T^γ	$M_{ee\gamma}$	M_{ee}	$P_T^{ee\gamma}$	E_T^{e1}	E_T^{e2}	η^γ	η^{e1}	η^{e2}
161555	619905	CP	83	381	93	9	35	56	-0.9	0.4	2.2

Table 24: The highest $M_{ee\gamma}$ $Z\gamma$ event

Figure 38 and 39 show the COT view and calorimeter tower view of this event.

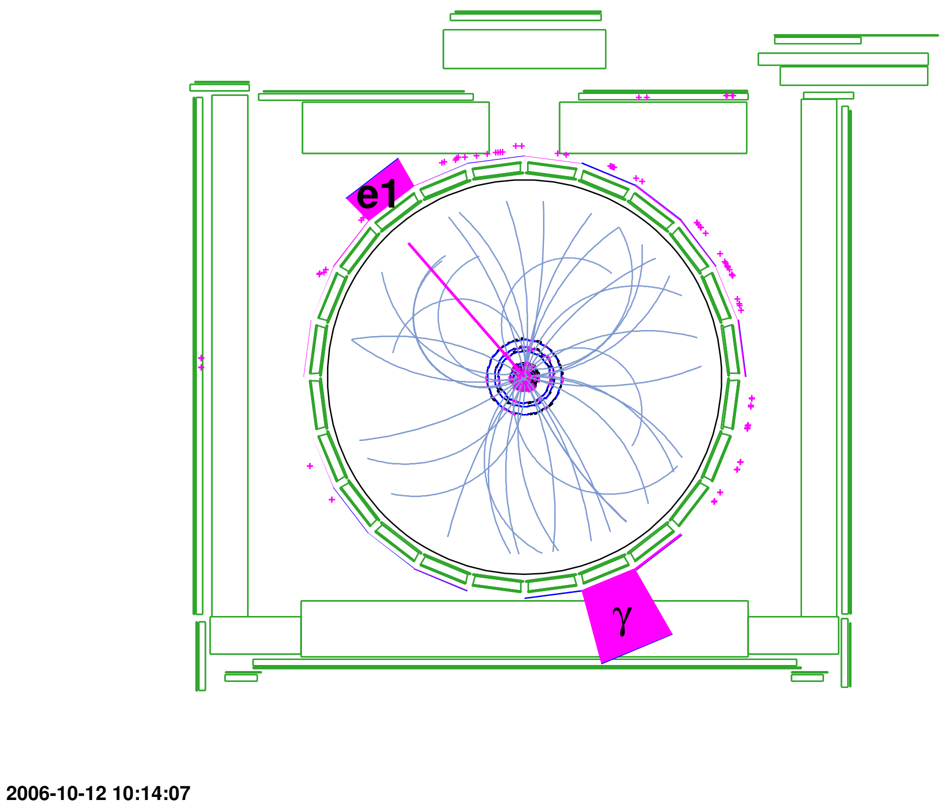

Figure 38: The COT view of the highest $M_{ee\gamma}$ event, event 619905 in run 161555.

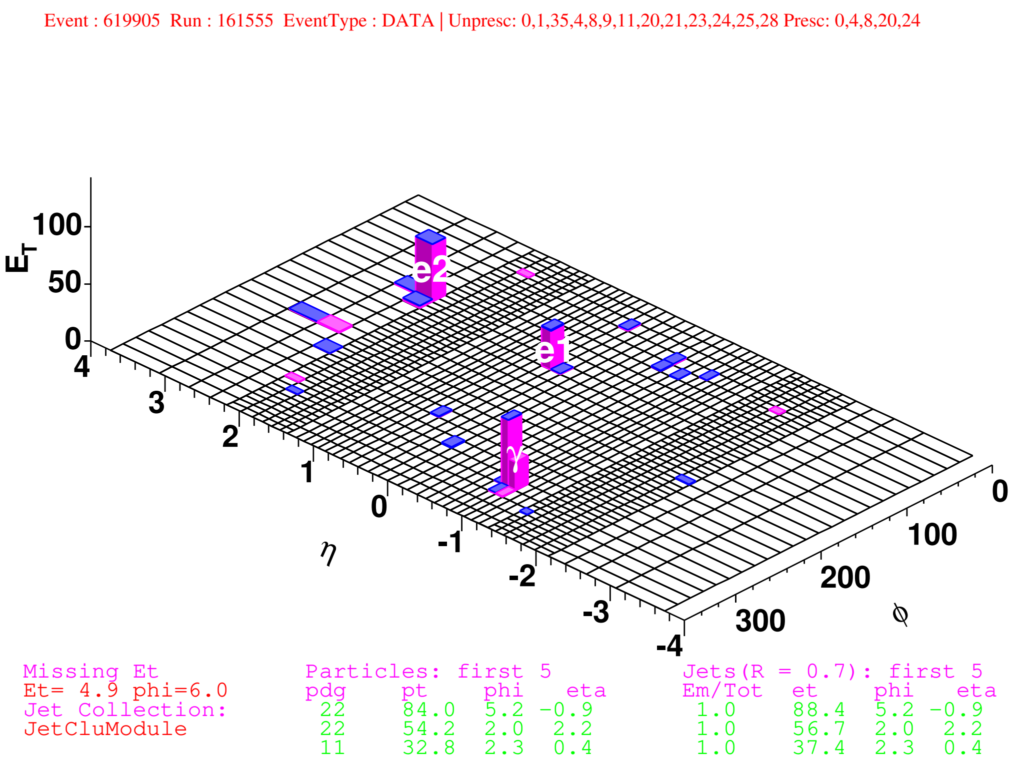

Figure 39: The calorimeter tower view of the highest $M_{ee\gamma}$ event, event 619905 in run 161555. Tower Et > 0.5 GeV.

10.6.3 The Highest $P_T^{ee\gamma}$ Event

Event 3732149 in run 162857 has the highest $P_T^{ee\gamma}$ (=142GeV/c).

The kinematic of this event is as following:

Run	Event	Z Type	E_T^{γ}	$M_{ee\gamma}$	M_{ee}	$\not{E}_T$	$P_T^{ee\gamma}$	E_T^{e1}	E_T^{e2}	η^{γ}	η^{e1}	η^{e2}
162857	3732149	CC	10	88	44	42	142	101	46	0.21	- 0.97	-0.33

Table 25: The highest $P_T^{ee\gamma}$ event

Figure 40 and 41 show the COT view and calorimeter tower view of this event.

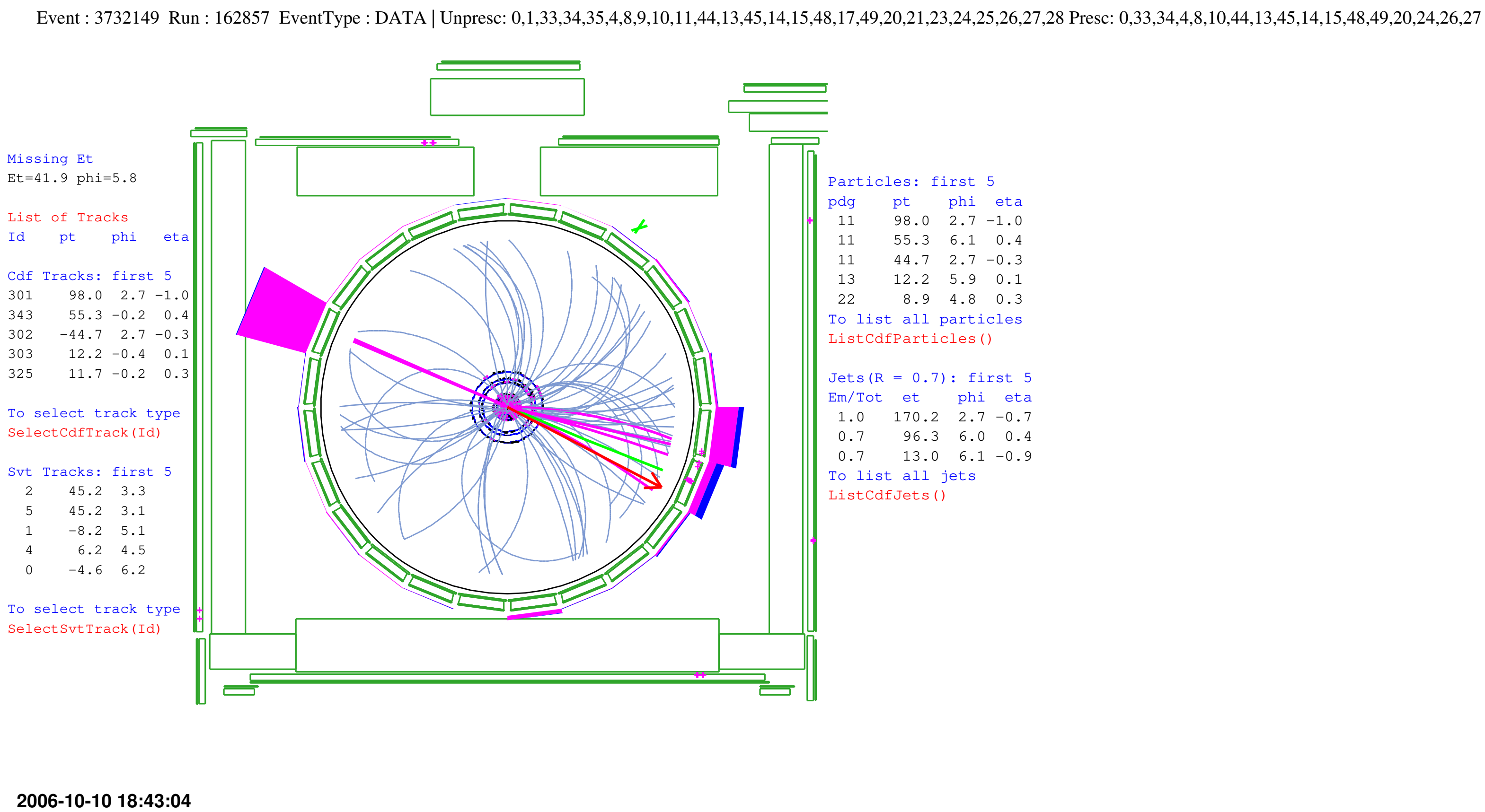

Figure 40: The COT view of the highest $P_T^{ee\gamma}$ event, event 3732149 in run 162857 .

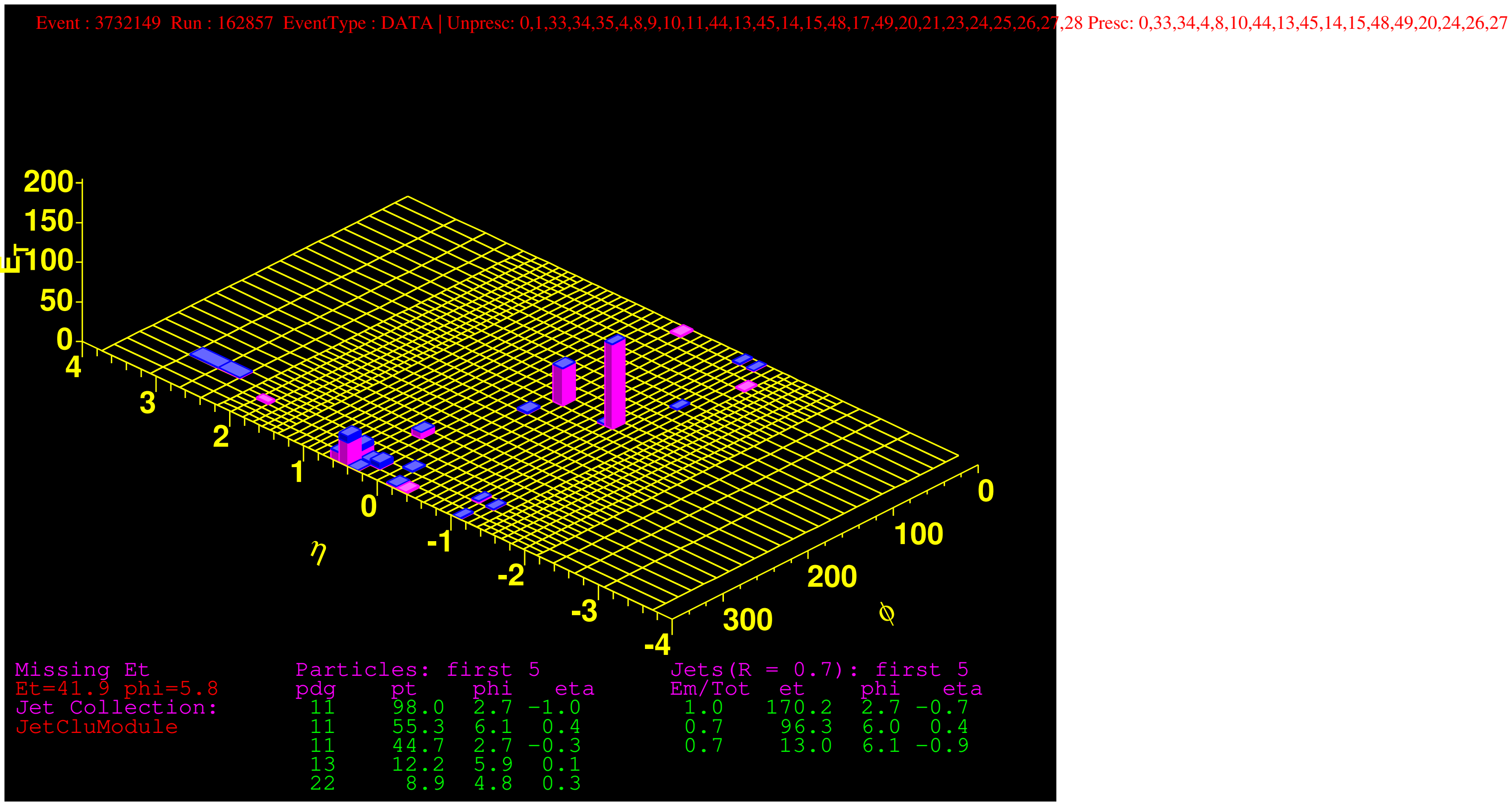

Figure 41: The Tower view of the highest $P_T^{ee\gamma}$ event, event 3732149 in run 162857 .

10.6.4 A Very High M_{ee} Event

Event 5975330 in 186048 run has a very high M_{ee} (=251GeV/c^2).

The kinematic of this event is as following:

Run	Event	Z Type	E_T^γ	$M_{ee\gamma}$	M_{ee}	$P_T^{ee\gamma}$	E_T^{e1}	E_T^{e2}	η^γ	η^{e1}	η^{e2}
186048	5975330	CP	19	269	251	60	64	83	0.5	-1.05	1.3

Table 26: The very high M_{ee} $Z\gamma$ event

Figure 42 and 43 show the COT view and calorimeter tower view of this event.

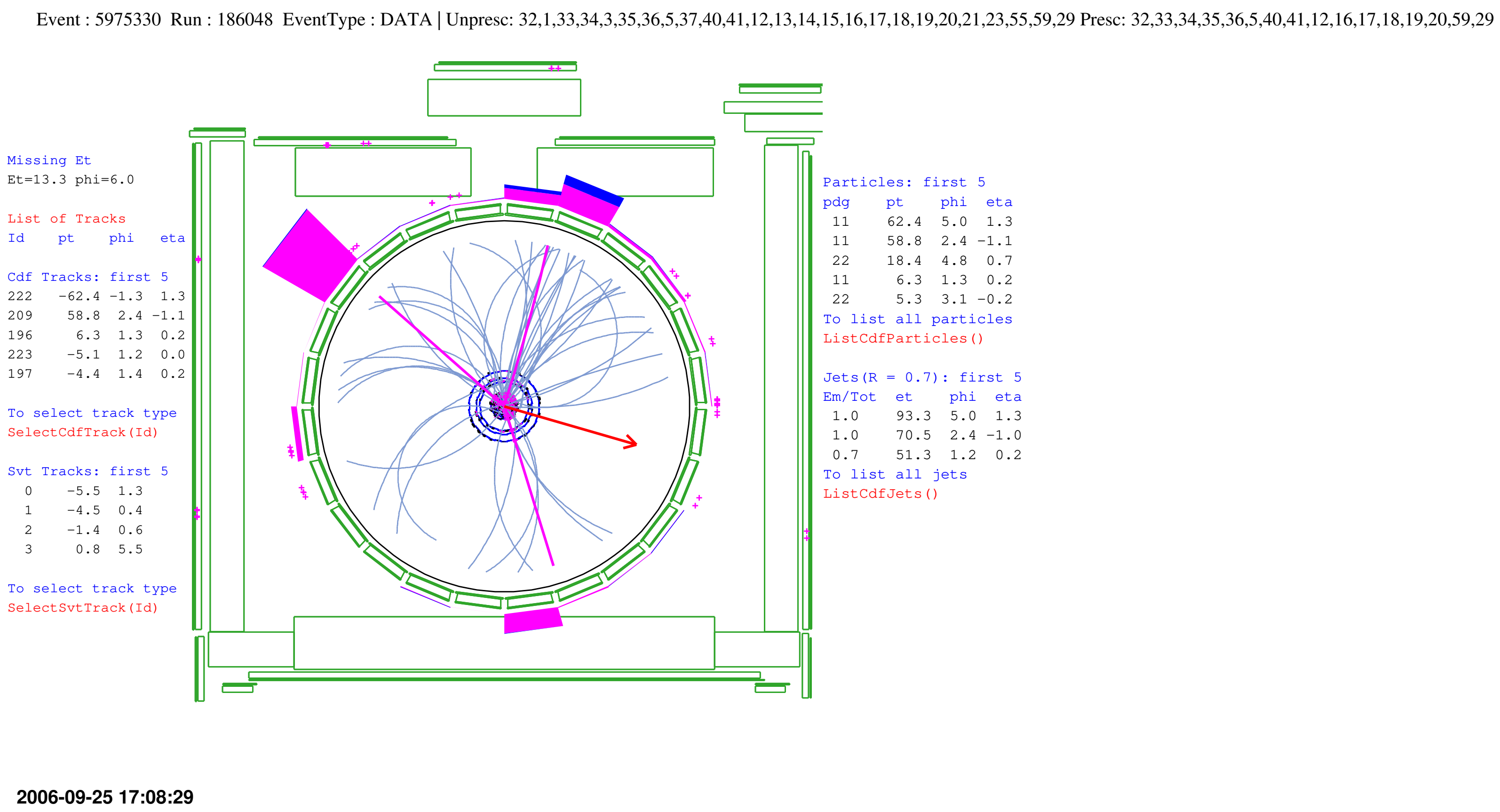

Figure 42: The COT view of a very high M_{ee} event, event 5975330 in run 186048.

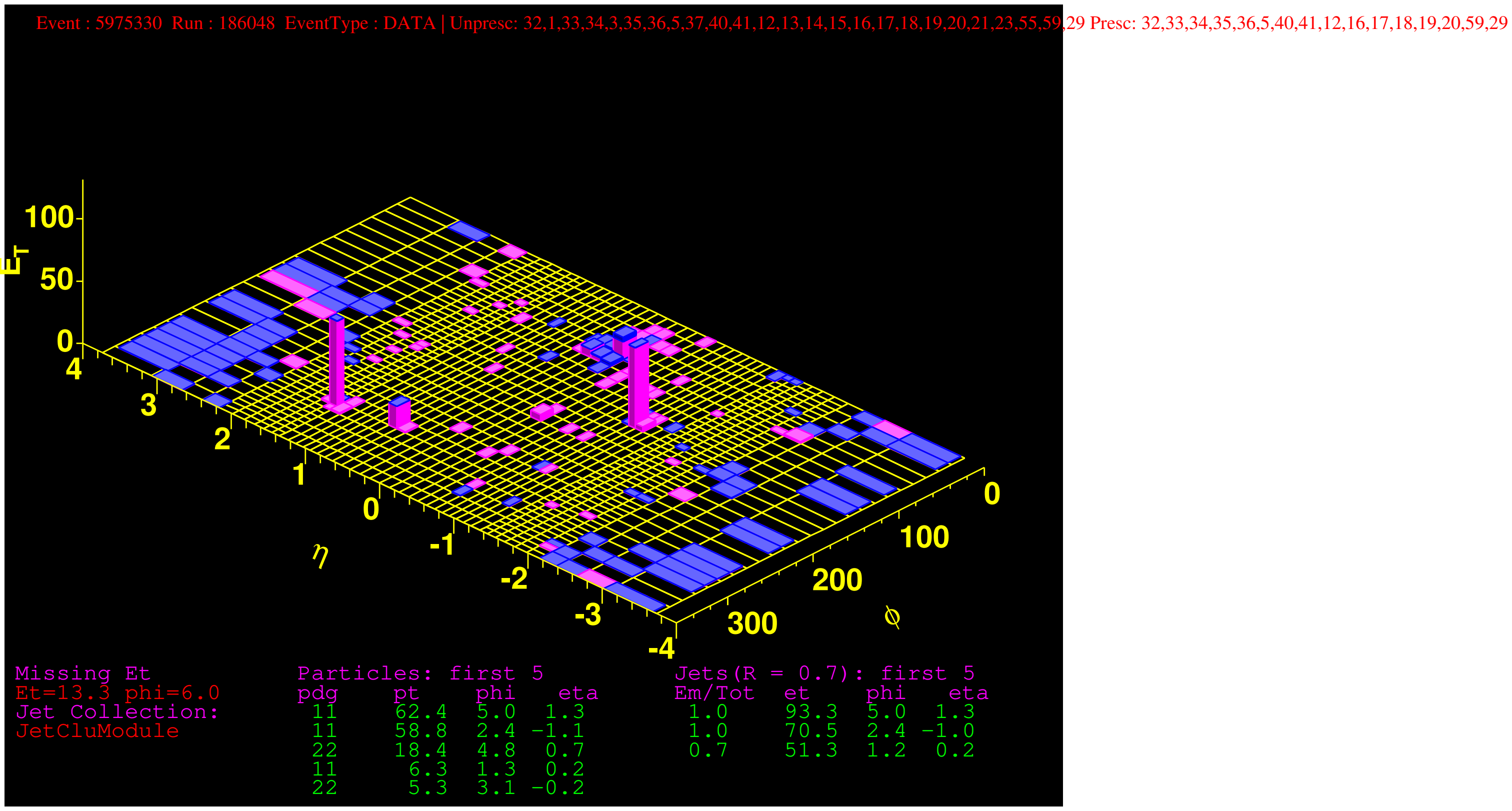

Figure 43: The calorimeter tower view of a very high M_{ee} event, event 5975330 in run 186048.

11 $Z\gamma$ Measurement in Muon Channel

11.1 $Z\gamma$ Event Counts

The $Z\gamma$ Events counts from 1.03fb^{-1} of data are listed in Tables 27 - 29.

Table 27: Central FSR photons in $Z \to \mu\mu$ events.

$\int \mathcal{L}dt(pb^{-1})$	1030
$\sigma_{NLO}(pb)$	3.3 ± 0.3
$Z\gamma$ type	FSR
Photon type	Central
N^{bkg}_{Z+jet}	2.4
N^{exp}_{SM}	136.9
N^{obs}	137

Table 28: Central ISR photons in $Z \to \mu\mu$ events.

$\int \mathcal{L}dt(pb^{-1})$	1030
$\sigma_{NLO}(pb)$	1.4 ± 0.1
$Z\gamma$ type	ISR
Photon type	Central
N^{bkg}_{Z+jet}	4.8
N^{exp}_{SM}	54.1
N^{obs}	56

Table 29: Central ISR + FSR photons in $Z \to \mu\mu$ events.

$\int \mathcal{L}dt(pb^{-1})$	1030
$\sigma_{NLO}(pb)$	4.7 ± 0.4
$Z\gamma$ type	FSR + ISR
Photon type	Central
N^{bkg}_{Z+jet}	6.8
N^{exp}_{SM}	188.6
N^{obs}	190

11.2 $Z\gamma$ Event Kinematics in Muon Channel

The $Z\gamma$ event kinematics distribution plots are shown in figures 44 - 49. MC is scaled so the number of Pythia Z events matches the number of inclusive Z's found.

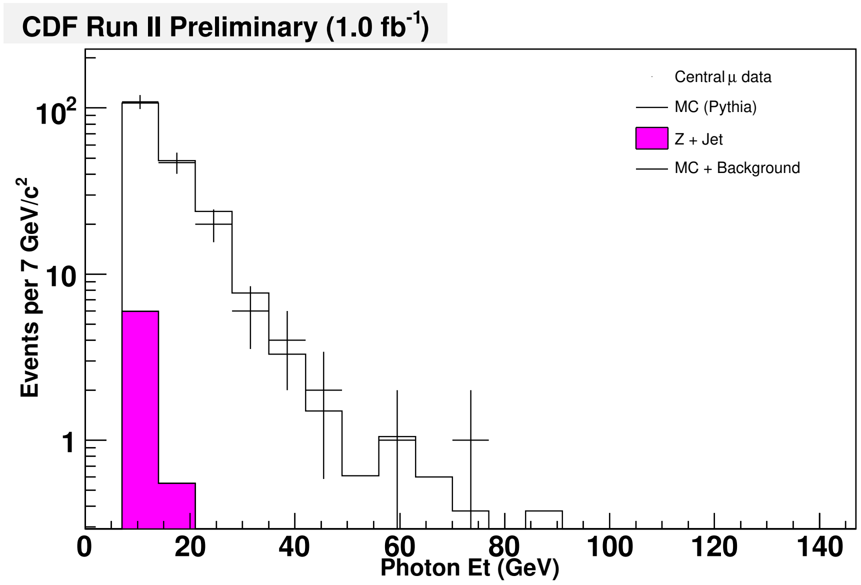

Figure 44: Photon Et Distribution in muon channel, bhel0d, 0h and 0i datasets, 7 GeV photon Et cut.

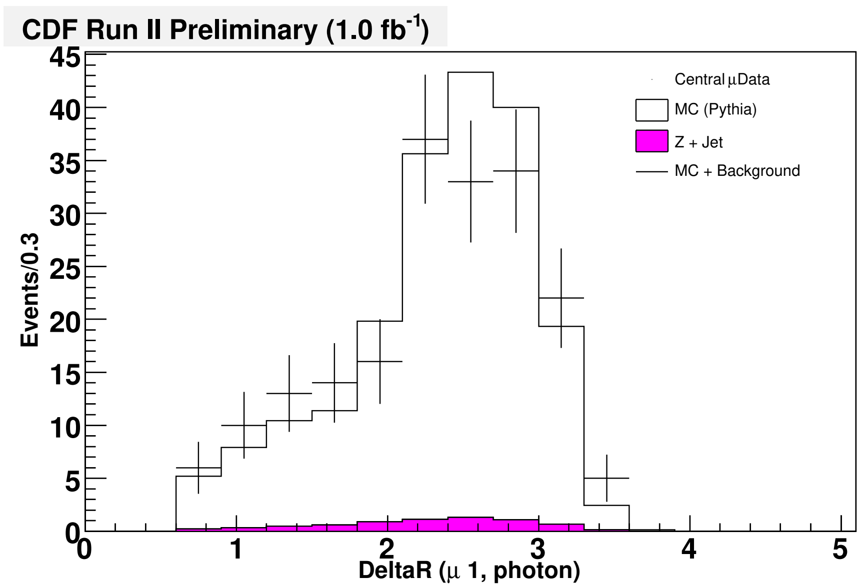

Figure 45: DeltaRa Distribution in muon channel, bhel0d, 0h and 0i datasets, 7 GeV photon Et cut.

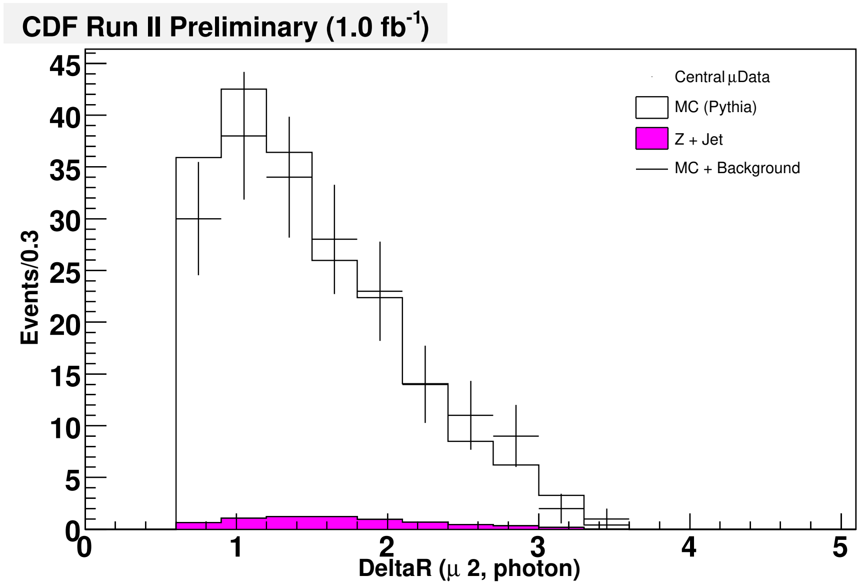

Figure 46: DeltaRb Distribution in muon channel, bhel0d, 0h and 0i datasets, 7 GeV photon Et cut.

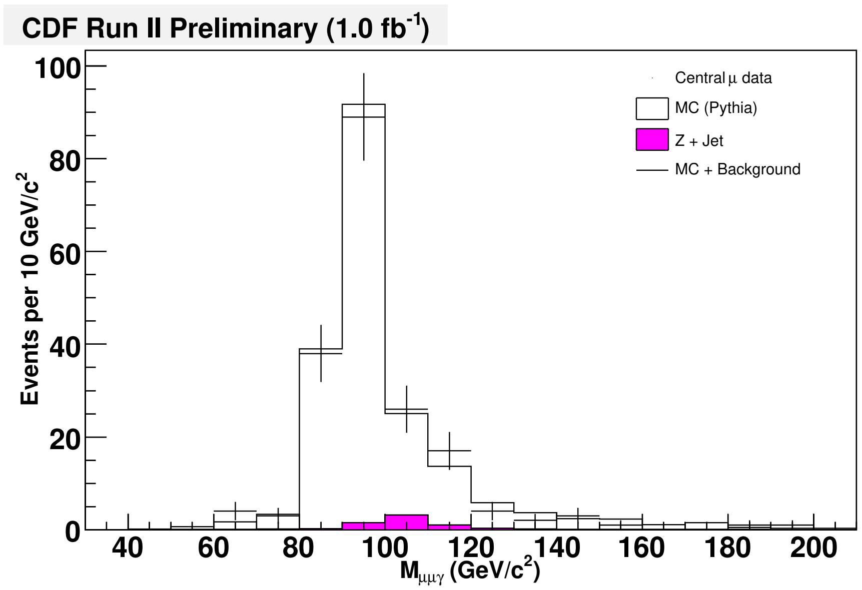

Figure 47: $M_{\mu\mu\gamma}$ Distribution in muon channel, bhel0d, 0h and 0i datasets, 7 GeV photon Et cut.

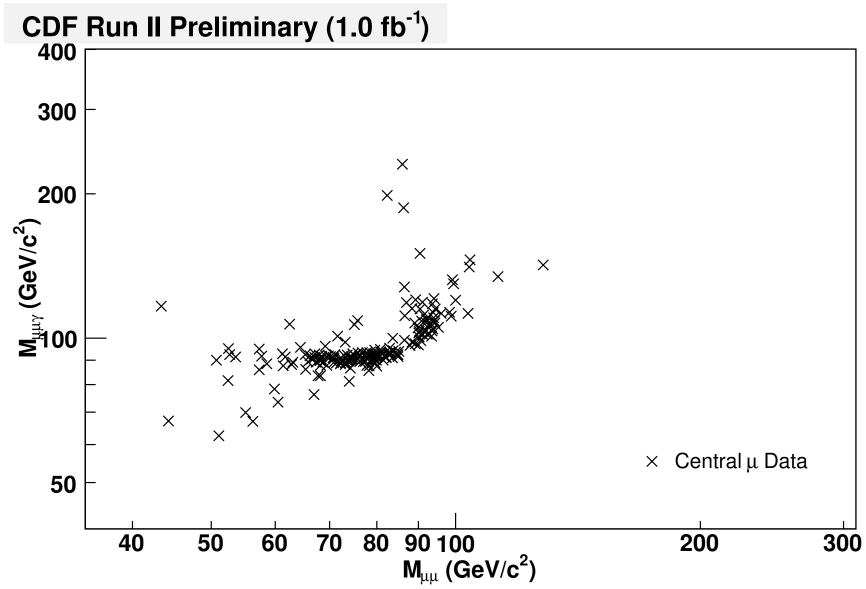

Figure 48: 2d Mass Distribution in muon channel, bhel0d, 0h and 0i datasets, 7 GeV photon Et cut.

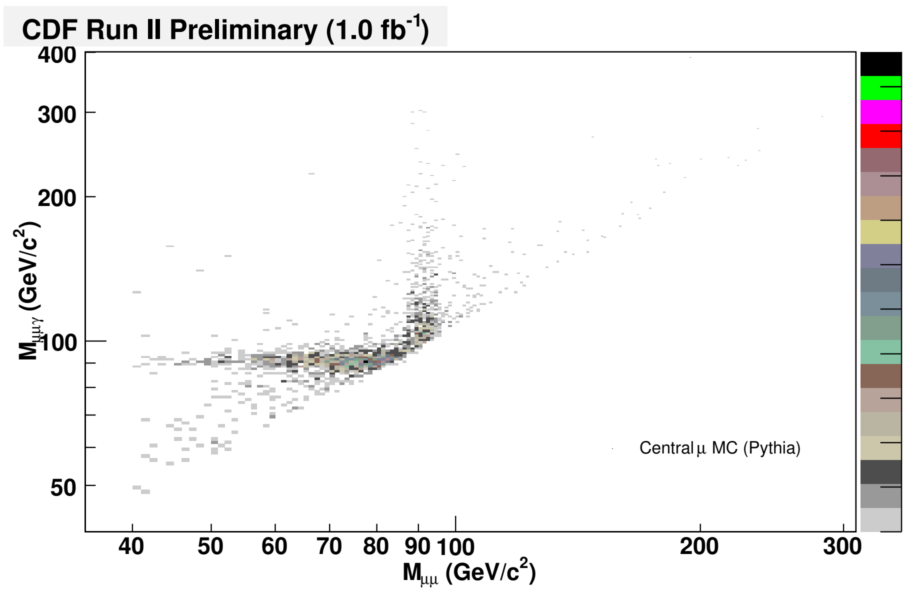

Figure 49: 2d Mass Distribution in muon channel, bhel0d, 0h and 0i datasets, 7 GeV photon Et cut.

12 Summary

We measure the $Z\gamma$ cross section in the electron channel. With 1fb^{-1} of data, 390 $Z\gamma$ events are observed, compared to the SM prediction of 367 events. The loose Z selection criteria doubles the $Z\gamma$ acceptance obtained in the previous $200pb^{-1}$ analysis. The measured cross section is 4.9 ± 0.3 (stat.) $\pm$ 0.3 (sys.) $\pm$ 0.3 (lum.) pb, compared to the theoretical prediction of 4.7 ± 0.4 pb. The kinematic distributions are compared to the SM predictions. There is generally good agreement with the SM predictions.

13 Acknowledgments

We would like to thank Chris Hays, Elliot Lipeles for useful comments and advice on the $Z\gamma$ measurement. Thanks to Dean Hidas for help on the Duke Ntuple codes. Thanks to Shih-Chieh Hsu for generating the Baur Zg MC samples. Thanks to Uli Baur for all helps on the ZGAMMA MC program.

References

[1] J. Deng et al., *Z Selection in Z + X Analysis*, CDF note 8505.

[2] T. Phillips et al., *Z ($\mu\mu$) Selection in Z + X Analysis*, CDF note 8758.

[3] H. Hayward, *Measurement of $Z^0\gamma$ Production in $p\bar{p}$ Collisions at $\sqrt{s} = 1.96$ TeV*, CDF note 7996.

[4] U. Baur et al., *Probing the weak-boson sector in $Z\gamma$ production at hadron colliders*, Phys. Rev. D 47, 4889(1993).

[5] R. Culbertson et al., *Pythia Settings for Generating $W\gamma, Z\gamma, W\gamma\gamma, Z\gamma\gamma$ Monte Carlo. SM Matching*, CDF note 8126

[6] Joint Physics baseline cuts for high Pt photons(v2.3), *http://www-cdf.fnal.gov/internal/physics/photon/docs/cuts.html*.

[7] S-M Wynne, *Very High-Pt Photon Efficiency Scale Factors V.2*, CDF note 7947, V2.0.
4, 9, 12, 14, 18 4, 6, 7, 14, 17, 19 4, 5 5 7 11, 12